

# The Oxygen Evolution Reaction on Passive Oxide Covered Transition Metal Electrodes in Aqueous Alkaline Solution. Part 1-Nickel

Michael E. G Lyons\*, Michael P Brandon

Physical and Materials Electrochemistry Laboratory, University of Dublin, Trinity College, Dublin 2, Ireland

\*E-mail: [melyons@tcd.ie](mailto:melyons@tcd.ie)

Received: 17 October 2008 / Accepted: 4 November 2008 / Published: 17 November 2008

---

Various aspects of the oxygen evolution reaction (OER) at passive oxide covered polycrystalline Ni electrodes in aqueous alkaline solution were investigated using electrochemical techniques. Steady state polarisation and electrochemical impedance spectroscopy (EIS) were used to measure kinetically significant parameters including the Tafel slope and the reaction order with respect to OH<sup>-</sup> activity. While reproducible values of the Tafel slope were readily observed, the recorded current density at a given applied potential displayed considerable variability over the course of a number of polarisation experiments, rendering difficult the extraction of the experimental reaction order parameter. This problem was resolved by applying relatively mild electrochemical pre-treatment routines to the working electrode. Cyclic voltammetry was used to probe the important issue of the interplay between the nickel oxy-hydroxide surface electrochemistry and the activity of the electrode for the OER. A current transient decay method was employed to estimate the electrode roughness factor. Amongst the mechanistic pathways proposed for the OER in the literature, only two are consistent with the experimental results reported here. The relative merits of these two pathways are discussed and the most likely is identified. The well known Krasil'shchikov mechanism is not suggested.

---

**Keywords:** oxygen evolution electrocatalysis, oxidized nickel electrodes, transition metal electrochemistry, oxygen evolution mechanisms

## 1. INTRODUCTION

The oxygen evolution reaction (OER) is the anodic reaction that accompanies, in aqueous electrolytes, commercially important cathodic processes such as metal electrowinning and hydrogen production via alkaline water electrolysis. For the latter process, the anodic overpotential is the major factor in limiting operational efficiency [1]. The optimal oxygen evolution anode materials are RuO<sub>2</sub>

and IrO<sub>2</sub>, since these oxides exhibit the lowest overpotentials for the reaction at practical current densities. The high cost of these materials and their poor long term stability in alkaline solution, renders their widespread commercial utilisation both uneconomical and impractical [2]. Nickel and its alloys have therefore become the anodes of choice for water electrolysis [1,2]. Although the OER overpotential is higher than for RuO<sub>2</sub> or IrO<sub>2</sub>, nickel based electrodes are relatively inexpensive and display excellent corrosion resistance in aqueous alkaline media, and thus offer an attractive compromise solution. That said, the OER electrocatalytic performance of metallic Ni (actually passive oxide covered Ni) in alkaline solution diminishes markedly with time [3].

In view of the aforementioned considerations, there has been, over the past thirty years, extensive research focussed on the development of OER electrocatalysts that display a combination of the desired characteristics of long term physical and chemical stability, satisfactorily low reaction overpotential and viable cost. Amongst the most promising materials that have been forwarded as OER anodes are, various inter-metallic alloys (often containing significant amounts of Ni, Co or Fe), electrodeposited Ni (NiO<sub>x</sub>) and Co (Co<sub>3</sub>O<sub>4</sub>) oxides, and mixed oxides, including spinels (particularly nickelites, cobaltites and ferrites) and perovskites.

While the relatively high activity of nickel hydroxide electrodes for the OER is welcome in alkaline electrolyser applications, it is a drawback where this material is utilised as the positive electrode in secondary alkaline batteries (e.g. Ni-Cd, Ni-MH and Ni-MH<sub>2</sub>) since it facilitates “self discharge” and consequently leads to a decrease of charge storage capacity [4,5]. Thus in contrast to electrolyser anode research, work in the battery area has been directed towards increasing the OER overpotential at nickel hydroxide electrodes. This has been achieved by the addition of cobalt hydroxide to the nickel hydroxide [6], however, depending on the amount of incorporated Co, this procedure can actually improve OER catalytic activity [7].

The most commonly proposed OER pathway for Ni oxides, Co oxides and mixed oxides of these two metals is that due to Krasil'shchikov [8] (or slight modifications thereof), originally devised for the reaction at Ni anodes and outlined below:



Here, S represents a catalytically active site for the OER. It has long been known [9], that even for metallic electrodes (like the polycrystalline Ni anodes considered in the present article), oxygen evolution always occurs on an oxide surface.

In reviewing the literature, we have formed the impression, that the popularity of this type of mechanism may be somewhat attributable to the fact that it was favoured by Hoare [9] in his influential 1968 work on oxygen electrochemistry (which was effectively the standard reference on the OER until the work of Kinoshita [2] in 1992) and was subsequently adopted by Lu and Srinivasan [3] and Bronoel and Reby [10] in often cited studies on the reaction at Ni electrodes in aqueous alkaline solution. Examples of more recent OER studies (with various electrode materials) that cite one or

more, of the three aforementioned references when making mechanistic assignments based on Tafel slope data, include the works of Bocca et al.[11], Wang et al. [12], Zhang et al.[13] and Fundo and Abrantes [14]. While it is accepted that mechanistic pathway determination may not have been the principal objective of these works, it must be commented that it is generally unsatisfactory to propose a reaction scheme on the sole basis of the experimental value of a single kinetic parameter such as the Tafel slope,  $b$ . A very useful summary of diagnostic criteria for five of the most commonly proposed pathways for the OER has been provided by Bockris and Otagawa [15] – examination of this shows that, in general, a given value of  $b$  may be indicative of rate control by a component step in any of several distinct pathways. A greater level of discrimination can be achieved by the experimental determination of the electrochemical reaction order with respect to  $\text{OH}^-$  activity,  $m_{\text{OH}^-}$ , associated with a given straight-line Tafel region. In this case the theoretical and experimental values of both  $b$  and  $m_{\text{OH}^-}$  must be in agreement, before a given pathway with an envisaged rate-determining step (RDS) can be admitted.

To the best of our knowledge the only systematic study of the variation, with  $\text{OH}^-$  activity, of the steady state current density at constant oxygen evolution overpotential for a nickel electrode, is that due to Bronoel and Reby [10]. However, as will be discussed later in this article, we have reservations about the conclusions of these authors. In contrast to Ni there have been relatively few investigations of the kinetics of the OER for polycrystalline Co and (especially) Fe electrodes in alkaline media. In view of the possible significance of such work in understanding the oxygen evolution behaviour of oxides (and mixed oxides) of these three metals, and indeed due to its intrinsic scientific interest in the area of electrocatalysis, we have conducted an extensive investigation of the OER at passive oxide covered Ni, Co and Fe surfaces. With the exception of the rather limited early work of Scarr [16], this is the first time that the OER, at electrodes of these three adjacent transition metal elements, has been studied with consistent methodology in the same laboratory. In this, the first of a three part series, the data obtained for Ni anodes is presented and discussed. In the second instalment consideration will be given to the OER at Co electrodes. The series will conclude with a treatment of the reaction at Fe anodes, and a comparative discussion of the oxygen evolution behaviour of the passive oxides of the three metals in aqueous alkaline solution.

## 2. EXPERIMENTAL PART

### 2.1. Electrode preparation and pre-treatment

The Ni electrodes were prepared from a 1mm thick polycrystalline nickel foil as supplied by Alfa Aesar (Johnson Matthey), purity 99.9945% (metals basis). Small sections of the metal were cut from the as-supplied foil, and filed to a size of 4mm  $\times$  4 mm (geometric surface area = 0.16 cm<sup>2</sup>), taking great care not to scratch the surface to be exposed as part of the electrode. The square piece of foil was then washed with copious de-ionised water, polished thoroughly with a slurry of 0.05 micron alumina powder, degreased with acetone, and washed again with de-ionised water. A length of copper wire was attached to the backside of the foil using a conductive epoxy as supplied by Circuit Works

(CW2400). After several days the square of foil was completely sealed into a glass tube (across the opening at one end) using epoxy (Araldite<sup>®</sup>). When the epoxy had completely hardened, it was polished back with fine abrasive paper until the 0.16 cm<sup>2</sup> area of metal was exposed. The newly exposed metal surface was polished successively with 1200 grit carbimet paper and an alumina slurry until a “mirror bright” finish was achieved.

Experiments were performed on Ni electrodes subjected to three different pre-treatment regimes. For clarity these will be referred to as electrode “types” A – C, where we define:

- Type A - A bright electrode was polished in a slurry of 0.05 micron alumina powder, rinsed in de-ionised water and then introduced to a cell containing 1.0 M NaOH, in which it was subjected to a potential cycle, initially in the anodic direction, between -0.8 and 0.675 V (vs. Hg/HgO) at 40 mVs<sup>-1</sup>.
- Type B - A bright electrode was polished as for A, but was then *pre-reduced* at 0 V for a period of 5 minutes in 1.0 M NaOH. Following this the electrode was allowed to rest on open circuit for 10 minutes, before being cycled once between -0.5 V and 0.675 V at 40 mVdec<sup>-1</sup> (anodic direction first).
- Type C - A bright electrode was polished as before and then pre-reduced in 1.0 M NaOH at a cathodic potential of -1.2 V in the hydrogen evolution region for 1 minute. It was elected to perform this extreme reduction, since literature sources [17-19] have indicated that prior reduction at such low potentials leads to enhanced Ni(II)/ Ni(III) oxidation currents in subsequent voltammetry experiments. The electrode potential was then allowed to decay on open-circuit for 15 minutes. Following this, the electrode was *pre-oxidised* for 3 minutes at 0.465 V (in the potential region of the Ni(II) oxidation reaction) and then for a further 2 minutes at 0.885 V.

Following any of the pre-treatments, the electrode was placed, for several minutes, in a beaker containing an amount of the test solution, before being finally transferred to the electrochemical cell.

## 2.2. Electrochemical cell and solutions

Solutions of NaOH with concentrations between 1.0 and 5.0 M were used as electrolytes. These solutions were prepared from NaOH pellets (BDH AnalaR<sup>®</sup>, minimum 98% purity) using millipore water (resistivity > 18 MΩ cm). The OH<sup>-</sup> activity,  $a_{OH^-}$ , for each solution concentration was calculated using the literature value [20] for the mean ionic activity coefficient,  $\gamma_{\pm}$ , for an NaOH solution of that concentration. No excess salts were added to the electrolyte solutions. All experiments were conducted at 25 ± 1°C.

A conventional three electrode cell arrangement was utilised. A platinum wire electrode (CH Instruments, Inc. -catalogue number. CHI 115) was employed as the counter electrode. The reference electrode was a mercury-mercuric oxide (Hg/HgO) electrode as supplied by Radiometer Analytical (cat no. XR400). The equilibrium potential of the cell, Pt(H<sub>2</sub>)|NaOH(aq)|HgO|Hg is 0.926 V at 25°C [21, 22] . Since the equilibrium oxygen electrode potential is 1.229 V vs. the RHE<sup>23</sup>, it follows that

$E^0_{O_2}$  is 0.303 V vs. Hg/HgO in the same solution. It is common practice in the literature [24, 25] on the OER, to express potential in terms of the oxygen overpotential,  $\eta$ , when the reference electrode is a Hg/HgO electrode in the same solution as the working anode. Clearly, in this case  $\eta$  is related to the voltage  $E_{meas}$  measured on the Hg/HgO scale (at  $T = 298$  K) as follows:

$$\eta = E_{meas} - 0.303V \quad (1)$$

For the sake of consistency it was elected to use Hg/HgO, 1M NaOH, as the universal reference standard in this work – therefore all voltages are quoted against this reference electrode. When used in NaOH solutions of different concentrations, the potential of the Hg/HgO electrode was checked relative to a second Hg/HgO, 1 M NaOH electrode, both before and after the experiment. No significant potential drift was noted after such experiments, implying that the concentration of the NaOH in the reference electrode chamber remains effectively constant over the time scale of typical polarisation measurements (ca. 2 – 3 hours). In any case, the 1 M NaOH solution in the reference electrode, was changed regularly to ensure experimental consistency.

### 2.3. Electrochemical measurements

With the exception of roughness factor measurements (see below) all electrochemical data was recorded digitally using a Zahner Elektrik IM6 Impedance measurement unit interfaced to a personal computer. Despite its name this equipment facilitates the performance of a wide range of electrochemical experiments including cyclic voltammetry and steady state polarisation measurements. The latter measurements were performed by applying a “staircase” type potential-time function to the working electrode. With a small potential step height of 5 mV, it was found that a step width of 2 minutes was satisfactory for the achievement of a consistent (steady state) current. The uncompensated solution resistance was determined by the impedance method and accordingly the steady state polarisation plots were corrected for the  $iR$  drop. Unless otherwise specified, all values of current density are normalised with respect to the geometric surface area.

Electrochemical impedance spectroscopy (EIS) experiments were performed at various potentials, using a 10 mV peak to peak ac potential perturbation. At each selected potential, the EIS measurement was performed only when a steady state dc current had become established. The SIM module of the IM6 Thales software suite permitted the fitting of the raw EIS data to equivalent circuit models using a *complex non-linear least squares* (CNLS) routine. A further useful feature of the SIM software is its *Kramers-Kronig rule check* option. All recorded impedance data were subjected to this consistency check, and rejected if they failed the test.

### 2.4. Active surface area estimation

Electrode roughness factors were estimated using the so-called  $OH_{ads}$  desorption method originally developed by Ho and Piron [26, 27]. The theoretical principles of this method will be

discussed later, however from an experimental viewpoint the technique involved the recording of the electrode current decay transient, following the interruption of a galvanostatically imposed current corresponding to the OER proceeding in the steady state. For each electrode this procedure was performed for a number of values of current density,  $i$ , derived from the steady state  $i(\eta)$  characteristic for that system.

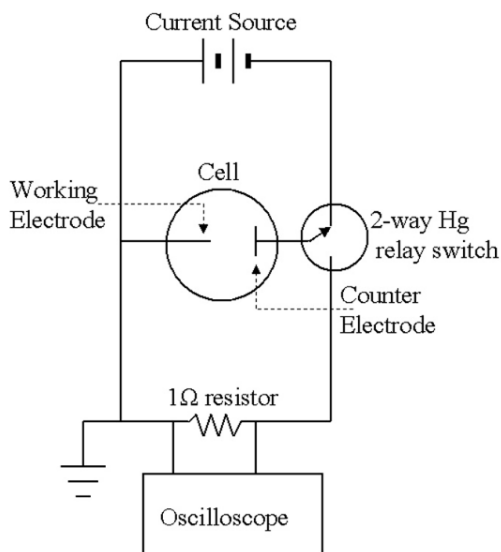


**Figure 1.** Basic circuitry used in the transient decay method of surface area estimation.

A schematic diagram of the basic measurement circuit is presented in Fig. 1. The current source was the IM6 rig operating in its galvanostatic mode. The oscilloscope was a Velleman PCS100 pc controlled digital storage oscilloscope. Owing to Ohms law, the instantaneous magnitude of the decay current through the  $1\ \Omega$  series resistor is obviously equal to the magnitude of the voltage across the resistor at that particular moment. Thus for a  $1\ \Omega$  resistor, and a  $1\ \Omega$  resistor only, the oscilloscope trace effectively maps the decay current–time ( $i$ - $t$ ) transient. The  $1\ \Omega$  series resistance was provided by a Levell R701 Resistance Box. The quantity measured using this apparatus was the total charge,  $Q_{dec}$ , passed in the course of the decay process, which was evaluated by integrating the digitally recorded oscilloscope  $i$ - $t$  trace between  $t = 0$ , and the time at which the decay current became zero.

### 3. RESULTS AND DISCUSSION

#### 3.1. Brief review of Ni (oxy-)hydroxide electrochemistry

As commented by Gottesfeld and Srinivasan; “the “science” of the OER is a “science” of the oxides and their properties” [28]. This will be shown to be very true in the case of the catalytic surface for the OER on Ni electrodes, and therefore a brief review is now presented on the extensive area of the electrochemistry of nickel hydroxides and oxyhydroxides.

Upon the immersion of a freshly polished Ni electrode in aqueous alkaline solution, a film of the hydrous Ni(II) oxide species,  $\alpha$ -Ni(OH)<sub>2</sub>, is spontaneously formed [18, 19, 29]. With ageing (especially in more concentrated alkali solution) the  $\alpha$ -Ni(OH)<sub>2</sub> can dehydrate and recrystallise as a largely anhydrous phase, denoted as  $\beta$ -Ni(OH)<sub>2</sub>. Of more interest in the present article is the composition of the passive oxide film formed by the oxidation of the aforementioned nickel hydroxides, since the redox transition of Ni(II) to higher oxidation states occurs at potentials immediately below those associated with significant OER current densities. It is this transition that is involved in the charging and discharge of nickel hydroxide battery electrodes and it has therefore received extensive research attention over many years – for topical reviews, see, for example, references 30 and 31. It should be noted that much of our knowledge in this area is derived from studies on electroprecipitated nickel hydroxide phases (most usually from nickel nitrate solutions onto Ni plaques [31]), however the same general principles are expected to apply to the passive oxide films formed on nickel electrodes in aqueous alkaline solution.

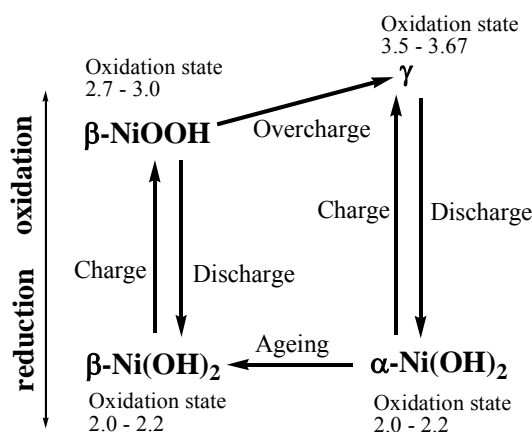


**Figure 2.** The Bode scheme for the Ni(OH)<sub>2</sub>/NiOOH redox transformation.

A major advance in the understanding of the Ni(II) → Ni(III) transition was made by Bode et al. [32] in 1966. These workers rationalised the redox switching behaviour of nickel hydroxide films in terms of four phases – see the cyclical scheme of Fig. 2. The non-stoichiometric nature of both the discharged and charged material is indicated by the average oxidation states of Ni in each phase. Bode et al. [32] envisaged that the oxidation of  $\alpha$ -Ni(OH)<sub>2</sub> to  $\gamma$ -NiOOH, would occur at a lower potential than the redox transition between the two  $\beta$  phases, a point that has been experimentally verified [32]. Indeed in his review of nickel hydroxides, Mc Breen [31] states that “all subsequent work has in general validated” the broad conclusions of the Bode model.

While there is general acceptance for the principles of the Bode model, it is important to understand that it is inappropriate to think about the formation of a compound or phase with a definite stoichiometry, during the complex Ni(OH)<sub>2</sub> to NiOOH transformation. Instead, the four phases of the Bode scheme should be considered as the limiting divalent and trivalent materials (tending towards tetravalent in the case of the  $\gamma$  phase) - the actual composition of the oxide at a given potential

depending on a range of factors including, its history, method of preparation, degree of hydration, concentration of defects etc. Nonetheless it is instructive to comment on what is known of the nature and structures of the four limiting model phases.

On the basis of powder neutron and X-ray diffraction studies [34], it is known that well crystallised  $\beta$ -Ni(OH)<sub>2</sub> adopts a brucite-type structure with layers of Ni(OH)<sub>2</sub> (the basal planes) perfectly stacked along the c-axis. The Ni(OH)<sub>2</sub> layers consist of a hexagonal planar arrangement of Ni<sup>2+</sup>-oxygen octahedra. As commented by McBreen [31] the nickel ions are all in the (0001) plane and are surrounded by six hydroxyl groups, each of which is alternatively above and below this plane. The unit cell parameter in the basal plane,  $a_0$ , was found to be 3.126 Å, the interlamellar distance,  $c_0$ , was determined as 4.593 Å, while 0.973 Å was reported for the O-H bond length [34].

The principal difference between the  $\alpha$ -Ni(OH)<sub>2</sub> and  $\beta$ -Ni(OH)<sub>2</sub> phases arises in the stacking of the planes along the c axis. An X-ray diffraction study on a sample of the former was conducted by Le Bihan and Figlarz [35]. They reported an interlamellar distance of ca. 8 Å and envisaged that the brucite like layers are misoriented with respect to each other. Furthermore they proposed that the expansion of the c-axis spacing, relative to that characteristic of the  $\beta$  phase, is due to the presence of water molecules and anionic species in the van der Waals gap, leading to the formation of a turbostratic phase.

It is difficult to make accurate determinations of the structures of the  $\beta$ -NiOOH and  $\gamma$ -NiOOH phases since they are amorphous materials [31], however it is generally accepted that they do display greater structural organisation than  $\alpha$ -Ni(OH)<sub>2</sub> [36]. In the case of  $\beta$ -NiOOH it is thought that the brucite structure is more or less maintained upon oxidation of  $\beta$ -Ni(OH)<sub>2</sub>. The unit cell parameters change to  $a_0 = 2.82$  Å and  $c_0 = 4.85$  Å [31]. From the point of view of electronic conductivity photoelectrochemical work [37,38] indicates that  $\beta$ -NiOOH is a much better conductor than its reduced form – it displays n-type conductivity with an estimated band-gap of ca. 1.75 eV [37]. This enhanced conductivity relative to Ni(OH)<sub>2</sub> and also the  $\gamma$  form of NiOOH (which contains more Ni<sup>4+</sup> - this forms an oxide of lower conductivity [2, 3]) is probably one of the reasons that that  $\beta$ -NiOOH is sometimes referred to as “*the right type of oxide*” [3] for the catalysis of the OER.

From the results of a series of charging and discharging experiments on various forms of Ni(OH)<sub>2</sub>, Barnard et al. [33] concluded that the  $\gamma$ -NiOOH phase has a higher Ni oxidation state of 3.3 – 3.67, compared to the oxidation state of  $\beta$ -NiOOH (2.7 – 3.0), owing to the presence of a relatively greater amount of Ni<sup>4+</sup> charge centres. Indeed, Aleshkevich et al. [39] estimated that less energy would be required to remove a proton from a hydroxyl group bonded to a Ni<sup>3+</sup> ion, than from one bonded to a Ni<sup>2+</sup> ion. On the basis of this they predicted that kinetic factors would favour the oxidation of Ni(II) to Ni(IV). This is an important point, since as commented by Briggs [30], it means that anodically prepared NiOOH will rarely be free from Ni(IV). Barnard et al. [33] took this concept a step further when they proposed that the required Ni oxidation state of 3.67 in their  $\gamma$  phase material could best be rationalised in terms of an empirical formula achieved by using a mixture of Ni<sup>2+</sup> and Ni<sup>4+</sup> cations rather than Ni<sup>3+</sup> and Ni<sup>4+</sup> cations, commenting that it “is easier to rationalise the development of the co-existing phases in the  $\alpha$ -Ni(OH)<sub>2</sub>/  $\gamma$ -phase system in terms of only one high valent species”.

### 3.2. Ni electrode 'type' A

Prior to the use of any freshly prepared polycrystalline Ni electrode in OER polarisation studies, it was subjected to series of potential cycling experiments, over the course of a number of days, to effectively "run it in". These experiments involved placing the electrode in 1.0 M NaOH solution, cycling its potential, four times (at  $40 \text{ mVs}^{-1}$ ), between  $-0.8$  and  $0.7 \text{ V}$ , before removing it from solution, polishing, rinsing and drying it (with soft tissue paper), and leaving for several hours before repeating the procedure (for a total of ten times). There was a progressive change in the voltammetric profile over the course of these experiments [40], which we considered, with reference to the literature [17, 18, 33, 41], to be a consequence of the active material becoming increasingly anhydrous with ageing. If the simple Bode scheme of Fig. 2 is admitted, this would correspond to a transition of material from the  $\alpha\text{-Ni(OH)}_2 \leftrightarrow \gamma\text{-NiOOH}$  cycle to the  $\beta\text{-Ni(OH)}_2 \leftrightarrow \beta\text{-NiOOH}$  cycle, owing to the gradual dehydration of  $\alpha\text{-Ni(OH)}_2$  to form the  $\beta$  phase. Given these intrinsic, progressive changes in the surface electrochemistry of the polycrystalline Ni electrode in alkaline solution, it was apparent to us that attainment of a reproducible Ni surface on which to conduct systematic OER studies was likely to present a significant challenge. This is especially true, considering that the voltammetric experiments described above, were conducted at less anodic potentials, and on a much shorter timescale than are required for steady-state polarisation measurements on the OER.

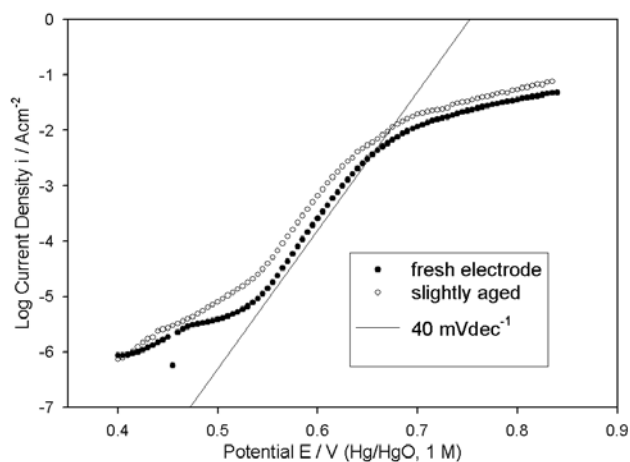


**Figure 3.** iR corrected steady state polarization curves recorded in the direction of increasing potential for 'type' A Ni electrodes in 3 M NaOH solution.

The results of the first and second steady state polarisation measurements on a freshly prepared "type" A Ni electrode in 3.0 M NaOH, are presented in Fig. 3. The voltammetric profiles corresponding to the pre-treatment potential cycles of the electrodes from which the data in Fig. 3 were obtained, are presented in Fig. 4. It is important to understand that all the data of Figs. 3 and 4 were obtained from the same electrode. For the polarisation curve denoted as "fresh electrode", this electrode was undergoing its first ever anodic polarisation, having been previously aged by a series of cycling experiments as outlined above.

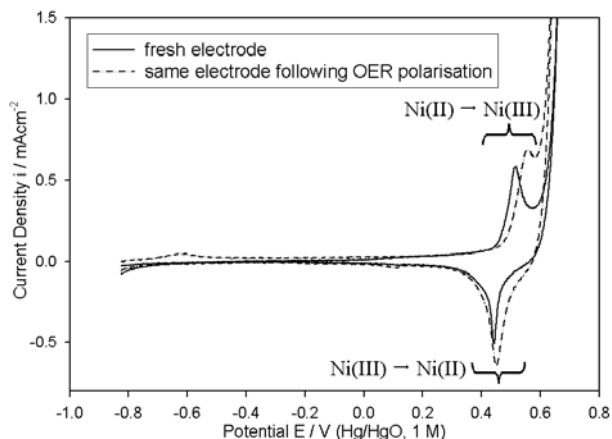


**Figure 4.** Pre-treatment CV's of the electrode surfaces on which the polarization data of figure 3 were obtained. The voltammograms were recorded in 1 M NaOH at a sweep rate of 40 mV/s.

The polarisation curve denoted as “slightly aged” in Fig. 3 is the result of the next steady state polarisation experiment on the same electrode. Following, the first polarisation, the electrode potential was allowed to decay for several hours on open circuit, the electrode was then removed, polished, and dried. The following day, the electrode was again subjected to pre-treatment regime A (see CV in Fig. 4) and subsequently the “slightly aged” polarisation curve was recorded in 3.0 M NaOH solution.

Examining Fig. 3, it is immediately apparent that the “slightly aged” electrode shows a significant enhancement of catalytic activity towards the OER in 3.0 M NaOH. As an example the recorded current density at a potential of 580 mV increases from 0.08 mAcm<sup>-2</sup> for the fresh electrode to 0.22 mAcm<sup>-2</sup> for the slightly aged electrode – an almost threefold increase. On the other hand, it would appear that the oxygen evolution mechanism remains the same – for both plots in Fig. 3, a Tafel slope of ca. 40 mVdec<sup>-1</sup> is observed at lower current densities.

The apparent reason behind the enhanced OER catalytic performance of the “slightly aged” Ni electrode is revealed by the cyclic voltammograms of Fig. 4. Calculating the active charge capacity associated with the Ni(II)↔Ni(III) transition,  $Q$  (characterised by integrating the cathodic voltammetric profile between its upper limit and ca. 0 V [17, 41]), it is found that for the fresh electrode,  $Q = 1.03$  mCcm<sup>-2</sup>. This increases by approximately 63% to 1.68 mCcm<sup>-2</sup> for the “slightly aged” electrode. Thus it would appear that the current density for the OER at a particular overpotential is proportional to the amount of active nickel oxide material. This effect was previously noted by Gennero De Chialvo et al. [41], who concluded that for nickel oxides of the *same type* (i.e.  $\alpha$ -Ni(OH)<sub>2</sub> or  $\beta$ -Ni(OH)<sub>2</sub>), this effect should be related to increasing surface roughness associated with the increasing amount of active material.

In the case of the voltammograms of Fig. 4, it is clear that not only has the charge capacity of the Ni electrode increased following its first OER steady state polarisation experiment, but the potentials of both the anodic and cathodic peaks have also increased. After Barnard et al.[33], it would seem reasonable to suggest that this is indicative of the presence of a higher proportion of the total material in the  $\beta$  –  $\beta$  cycle after the first steady state polarisation measurement at high anodic potentials

in 3.0 M NaOH, relative to the situation before this polarisation. If it is true that  $\beta$ -NiOOH is indeed the “right type of oxide” for the OER on Ni anodes, then it would be expected that the increased proportion of this material would also lead to enhanced catalytic activity towards the OER. It is therefore probable that the increased OER current densities of the “slightly aged” Ni electrode of Fig. 3 arise from a combination of physical effects owing to increased available surface area, and electrochemical effects due to an increased concentration of the more catalytically active form of nickel oxide. What is clear, is that the pre-treatment combination of mechanical polishing and a potential cycle in 1.0 M NaOH, is ineffective in restoring the initial fresh surface of the polycrystalline Ni electrode in a reproducible manner, following the relatively severe anodic polarisation associated with the steady state kinetic measurements.

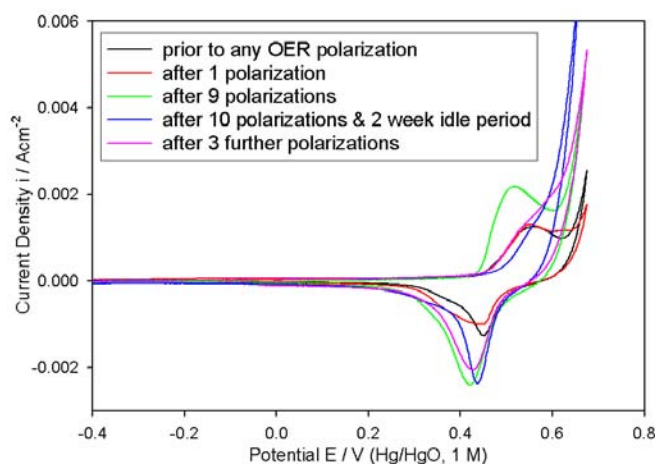


**Figure 5.** Pre-treatment cyclic voltammograms of the electrode surfaces on which the polarization data of figure 6 were obtained. The voltammograms were recorded in 1 M NaOH at 40 mV/s.

The difficulty in reproducing the initial surface state of a Ni electrode that had never been subject to polarisation at high oxygen evolution overpotentials, following the application of such a severe potential regime, was not altogether surprising. The possibility was however considered, that a sufficiently reproducible electrode surface might be attained following a number of steady state polarisation measurements accompanied by the pre-treatment routine A. To this end the results were reviewed, of a preliminary, unsuccessful attempt to obtain reproducible steady state polarisation curves on a different “A type” Ni electrode in solutions of NaOH ranging from 1.0 – 5.0 M, to examine whether the results of polarisation studies became more consistent, with an increasing number of such experiments. Several of the pre-treatment voltammograms from this set of experiments are depicted in Fig 5. The corresponding subsequent steady state polarisation curves, all recorded in 1.0 M NaOH, are presented in Fig. 6.

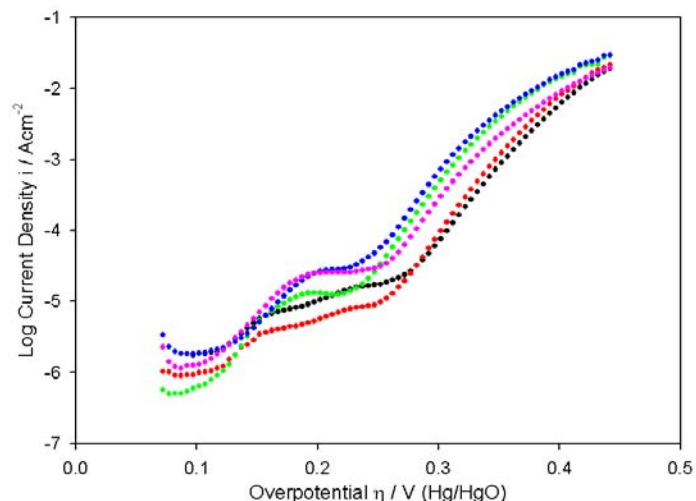


**Figure 6.** *iR* corrected steady state polarisation curves recorded in the direction of increasing potential for “type” A Ni electrodes in 1.0 M NaOH solution. Polarisation curves were recorded subsequent to the corresponding CVs in Fig. 5. <sup>a</sup>

It was found that the oxygen evolution overpotential at a given current density, initially decreased with ageing of the electrode – see the three earliest scans in both Figs. 5 and 6. Calculating the active charge capacities for earlier voltammograms yields;  $Q = \sim 3.65 \text{ mCcm}^{-2}$  for the previously unpolarised electrode,  $Q = \sim 4.00 \text{ mCcm}^{-2}$  for the electrode characterised the day after the first OER polarisation in 1.0 M NaOH, and  $Q = \sim 7.89 \text{ mCcm}^{-2}$  for the surface characterised after nine polarisation experiments. It is obvious that the progressive improvement in the OER catalytic activity of the electrode over the course of the three earlier polarisation measurements in Fig. 6 is related to the increased amount of active nickel oxide material, and therefore presumably increased catalytic surface area. Again this highlights the fact that mechanical polishing alone is ineffective in fully removing the anodic oxide formed on Ni in alkaline media. It would appear that a residual amount of oxide is resistant to removal by polishing, and indeed that the amount of this oxide increases progressively with use of the electrode in OER polarisation studies.

As is evident from Fig. 5, the voltammetric profile of the active Ni surface altered dramatically after a fortnight of electrochemical inactivity, during which time it was stored in dry conditions at room temperature. The charge capacity, as calculated by the integration of the cathodic peak, was found, in this case, to be  $Q = \sim 6.61 \text{ mCcm}^{-2}$ , as compared to  $Q = \sim 7.89 \text{ mCcm}^{-2}$  for the previous pre-polarisation CV, recorded two weeks previously. However the post-idle period electrode displayed somewhat greater activity for the OER, with a current density of  $0.73 \text{ mAcm}^{-2}$  at  $\eta = 302 \text{ mV}$ , compared to  $0.51 \text{ mAcm}^{-2}$ , recorded two weeks before. This observation would seem to defy the apparent existence of a proportionality between  $Q$  and the electrocatalytic activity towards the OER, noted for the Ni electrode in relation to the data of Figs. 3 and 4 and the earlier scans of Figs. 5 and 6, as well as by other workers [41].

This anomaly would appear to be related to the type of oxide that comprises the active material. It is evident that the peak potential on the cathodic profile has shifted in the positive direction by  $\sim 20$

mV, following the period of storage at ambient conditions. The onset of significant Ni(OH)<sub>2</sub> oxidation is also shifted in the positive direction, although clearly, the concept of an anodic peak potential is rather meaningless in the case of the post idle period CV of Fig. 5. Again referring to the work of Barnard et al. [33], this behaviour suggests that a greater proportion of the active material exists as the anhydrous form, following ageing in the air at room temperature for two weeks. Gradual ageing of  $\alpha$ -Ni(OH)<sub>2</sub> to  $\beta$ -Ni(OH)<sub>2</sub> is envisaged by the Bode scheme [32] and is widely accepted [31]. It is certainly not surprising that dehydration of the residual oxide should occur when the electrode is stored for some time under dry conditions. The increased activity of this electrode for the OER, after its idle storage period, despite the smaller value of  $Q$ , supports the conjecture [3] that  $\beta$ -NiOOH (or the oxidation product of  $\beta$ -Ni(OH)<sub>2</sub> at any rate) is the optimum type of oxide for the catalysis of the OER on a Ni electrode.

Following three further steady state polarisation experiments on successive days, the activity of the electrode decreased – the current density at  $\eta = 302$  mV, dropped back to 0.30 mAcm<sup>-2</sup> in the case of the latest polarisation curve of the series in Fig. 6. Referring to the corresponding voltammogram in Fig 5, it can be seen that this fall in catalytic activity, is related to reversion of a proportion of the oxide material to the  $\alpha - \gamma$  Bode cycle, as evidenced by a shift of the reduction peak profile back in the cathodic direction. This observation is in line with the prediction of the Bode scheme [32], that upon overcharge at high anodic potentials,  $\beta$ -Ni(III) material will be converted into the  $\gamma$  phase. Therefore, while aging transforms active material from the  $\alpha - \gamma$  cycle to the  $\beta - \beta$  cycle via dehydration of  $\alpha$ -Ni(OH)<sub>2</sub>, overcharging of the  $\beta$ -Ni(III) phase returns some of the oxide to the former cycle.

The foregoing discussion leads to following important qualitative conclusions regarding oxygen evolution at a polycrystalline Ni electrode in aqueous alkaline solution:

(a) it is very difficult to achieve a reproducible catalytic surface for the OER on Ni by mechanical polishing alone, since this is ineffective in removing all of the anodic oxide formed on the electrode during polarisation.

(b) the oxygen evolution catalytic activity of a given Ni electrode is dependent not only on the amount of redox active material (as quantified by  $Q$ ) but also on the nature of that material, i.e.  $\alpha - \gamma$  cycle vs.  $\beta - \beta$  cycle.

(c) in view of the above points, the key to achieving reproducible polarisation measurements would seem to lie in devising a more thorough pre-treatment routine than procedure A.

(d) it is clear from the polarisation curves of Figs. 3 and 6, that although the catalytic activity depends on the amount and composition of the active material, the mechanism of the OER, at lower current densities at any rate, remains the same, as is indicated by the observation of a constant Tafel slope of  $\sim 40$  mVdec<sup>-1</sup> in all cases.

In relation to points (c) and (d) it is worth commenting that, while the difficulty in achieving coincident steady state polarisation curves over the course of several experiments in the same electrolyte does not pose a problem in determining the Tafel slope, it is a issue in the experimental derivation of the OH<sup>-</sup> reaction order,  $m_{OH^-}$ , since the latter process involves the analysis of the

variation of the OER current density,  $i$ , at a given potential,  $E$ , with  $\text{OH}^-$  activity,  $a_{\text{OH}^-}$ . Obviously if a reproducible value of  $i$  is not attainable at a particular potential for constant  $a_{\text{OH}^-}$ , the accurate determination of  $m_{\text{OH}^-}$  for that potential is then impossible. Pre-treatment regimes B and C (see Experimental) were devised in an attempt to circumvent the aforementioned reproducibility issues.

### 3.3. Ni electrode 'type' B

Cyclic Voltammograms recorded in 1.0 M NaOH as the final part of pre-treatment routines B and C are presented in Fig. 7. These scans were performed on the same Ni electrode specimen, and also included is a CV characterising that electrode when it was freshly prepared (although subsequent to the "run-in" procedure mentioned previously). It was found that such CVs recorded as part of either pre-treatment regimes B or C were satisfactorily reproducible (i.e. the values of  $Q$  agreed to within <10% while the profiles were similar in appearance for electrodes subjected to the *same* type of pre-treatment) over the course of a series of 10 polarisation measurements. It is obvious that there is a significantly larger charge transfer associated with the  $\text{Ni}(\text{OH})_2 \leftrightarrow \text{NiOOH}$  redox transition ( $Q = \sim 1.57 \text{ mCcm}^{-2}$  for "type" B vs.  $\sim 4.99 \text{ mCcm}^{-2}$  for "type" C) in the case of electrode "type" C relative to "type" B.

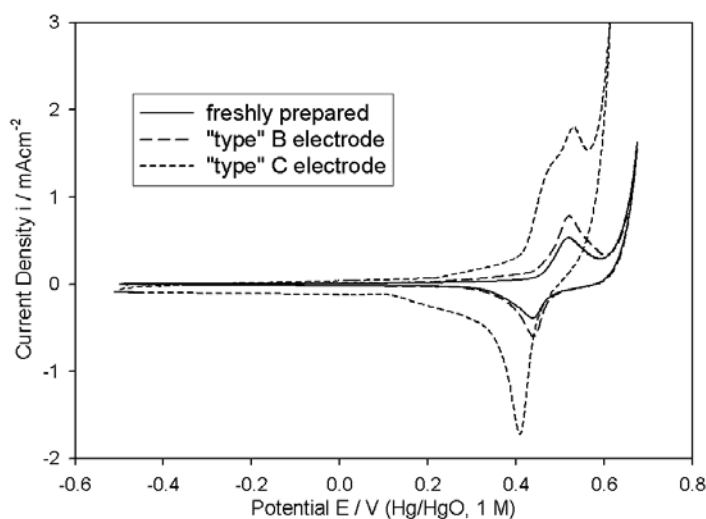


**Figure 7.** Typical pre-treatment CVs of the "type" B and C Ni electrodes, recorded in 1.0 M NaOH at a sweep rate of  $40 \text{ mVs}^{-1}$ .

An oxygen evolution steady state polarisation characteristic, recorded for a "type" B Ni electrode in 1.0 M NaOH solution is presented in Fig 8. The issue of the most appropriate direction for the recording of OER steady state polarisation curves is often overlooked in the literature. In the present work (as is the case for the data of Fig. 8) most steady state experiments have been conducted by progressing in the anodic direction for several hundred millivolts, from below the potential at which significant oxygen evolution currents are noted. The direction of the potential step program is then reversed, facilitating the monitoring of the OER from potentials at which it occurs at significant steady

state current density, down to the potential at which the net current becomes cathodic. The sweep direction then reverts to the direction of increasing potential. This approach enables the characterisation of the OER in both the situation where the fractional coverage,  $\theta$ , of reaction intermediates is expected to increase from low values towards unity (direction of increasing potential), and the opposite situation (direction of decreasing potential). Comparison of the 1<sup>st</sup> and 2<sup>nd</sup> forward scans also allows information to be obtained on the stability of the system with time. Reaction order data have generally been extracted from the first sweep in the direction of increasing potential, since the initial electrode surface condition, which has been manipulated by pre-treatment in 1.0 M NaOH to be as similar as possible for all NaOH solutions, is likely to be progressively altered depending on OH<sup>-</sup> concentration, as the experiment proceeds. Therefore reaction order data taken early in the course of the experiment are less likely to be affected by artefacts arising from the different rates of surface processes (such as oxide growth and possibly dissolution) occurring in hydroxide solutions of different concentration.

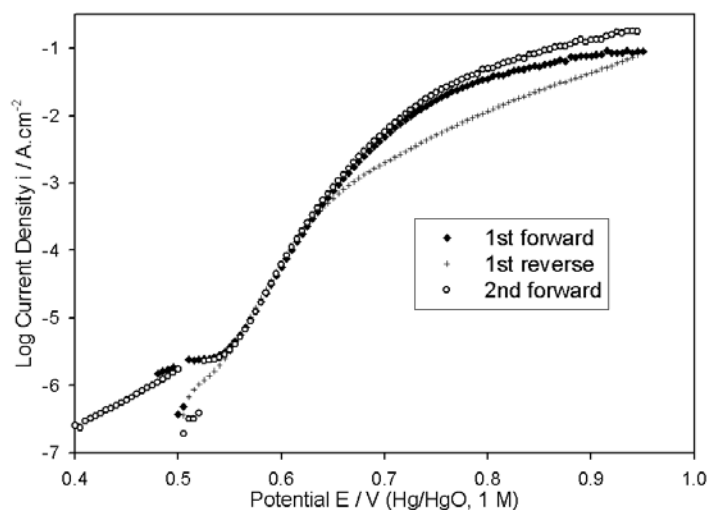


**Figure 8.** *iR* corrected steady state polarisation curve, recorded continuously in 1.0 M NaOH solution on a “type” B Ni electrode, initially in the direction of increasing potential (1<sup>st</sup> forward), then in the direction of decreasing potential (reverse), and finally in the direction of increasing potential for a second time (2<sup>nd</sup> forward).

The most notable feature of the bi-directional curve of Fig. 8 is the severe hysteresis at higher overpotentials between the forward direction and reverse direction scans. Indeed this hysteresis is also observed in the polarisation curves for the other hydroxide ion concentrations. Very few of the steady state polarisation experiments on oxygen evolution that have been reported in the literature (for electrodes of any material) have been conducted in both the directions of increasing and decreasing potential, and to the best of our knowledge, there has been little significant attempt to discuss the phenomenon of hysteresis sometimes observed in such measurements. The one exception is due to Kobussen et al. [42], who noted hysteresis at higher overpotentials in studies on the OER at both La<sub>0.5</sub>Ba<sub>0.5</sub>CoO<sub>3</sub> [43] and polycrystalline Co [24] electrodes in alkaline media. Like us, these workers observed that the activity of their electrodes for a given potential, was lower on a sweep in the

direction of decreasing potential, than on a prior sweep in the opposite direction. They proposed [42] that anodisation of the electrodes at higher oxygen evolution overpotentials (i.e. at potentials above those associated with the lower straight line Tafel region) leads to further passivation and a loss of activity for oxygen evolution. Whatever the underlying cause of the hysteresis, it would seem logical that more credence be attached in mechanistic analyses, to polarisation data in regions of potential, where the forward and reverse scans largely coincide, such as the  $40 \text{ mVdec}^{-1}$ , lower overpotential sector in the plot of Fig. 8.

A series of  $iR$  compensated steady state polarisation curves (first scan in the direction of increasing potential) for “type” B electrodes are presented in Fig. 9. A Tafel slope of  $\sim 40 \text{ mVdec}^{-1}$  is obvious at lower current densities across the entire studied range of NaOH solution concentrations, as was also the case with the slopes observed in Figs. 3 and 6 for “type” A electrodes. It should also be commented that, although an apparent straight-line Tafel region with a slope of ca.  $120 \text{ mVdec}^{-1}$ , is observed in the reverse sweep, at current densities immediately above the  $40 \text{ mVdec}^{-1}$  region, for the 1.0 M plot of Fig. 8, the slopes at similar overpotentials in the reverse scans for the solutions of other concentrations, tend to vary between approximately  $120$  and  $180 \text{ mVdec}^{-1}$ . Hence the extraction of kinetic parameters from this region of overpotential in the reverse direction scans might be a dubious enterprise, and therefore the matter is not pursued here.

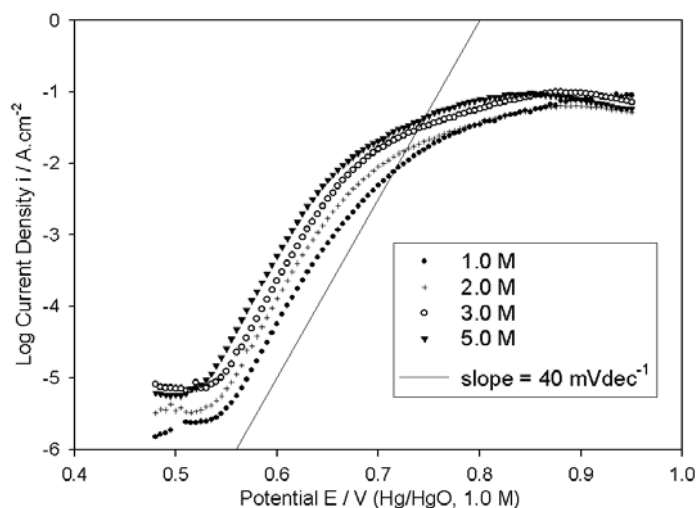


**Figure 9.**  $iR$  corrected steady state polarisation curves recorded in the direction of increasing potential for a “type” B Ni electrode in NaOH solutions of various concentration.

Reaction order plots ( $\log i$  vs.  $\log a_{\text{OH}^-}$  at a given value of  $E$ ) with respect to  $\text{OH}^-$  activity, were constructed, based upon the polarisation data of Fig. 9 in the low overpotential  $40 \text{ mVdec}^{-1}$  Tafel region. Two of these are presented in Fig. 10, indicating values of  $m_{\text{OH}^-} = (\partial \log i / \partial \log a_{\text{OH}^-})_E = 1.06$  at  $E = 0.58 \text{ V}$  and  $m_{\text{OH}^-} = 1.03$  at  $E = 0.6 \text{ V}$ . Similar slopes were observed for plots based upon the  $\log i(E)$  data for other potentials in this section of the polarisation curve. Overall it can be concluded that  $m_{\text{OH}^-} \approx 1$ , in the  $\sim 40 \text{ mVdec}^{-1}$  Tafel slope region for the “type” B Ni electrode.

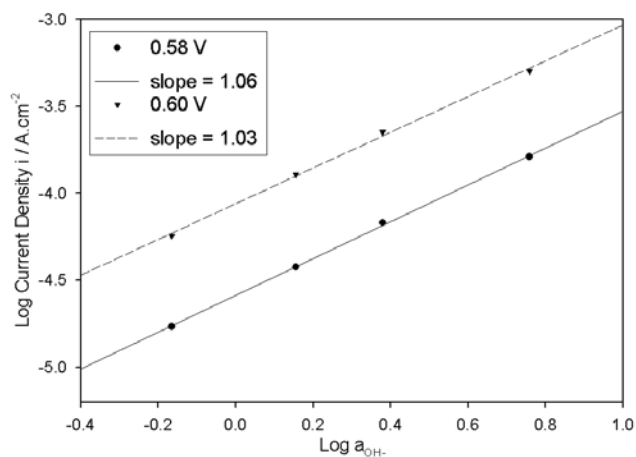


**Figure 10.** Reaction order plots based on the polarisation curves of Figure 9 for two values of potential in the  $40\text{mVdec}^{-1}$  Tafel slope region.

### 3.4. Ni electrode 'type' C

Steady state polarisation curves for Ni electrodes pre-treated according to regime C, are presented in Fig. 11. Again it is clear that the data in the lower overpotential region are characterised by Tafel slopes of approximately  $40\text{mVdec}^{-1}$ , although it is to be admitted that in case of the 5.0 M electrolyte, the  $40\text{mVdec}^{-1}$  slope is only truly observed over a limited potential range from  $\sim 0.525 - 0.555\text{ V}$ , with a slope of approximately  $30\text{mVdec}^{-1}$ , noted at lower current densities, altering to ca.  $50\text{mVdec}^{-1}$  directly above to  $40\text{mVdec}^{-1}$  region. Bi-directional measurements, revealed that hysteresis similar to that observed in Fig 8 for “type” B Ni electrodes, is also a characteristic of the steady state polarisation behaviour of “type” C Ni anodes.

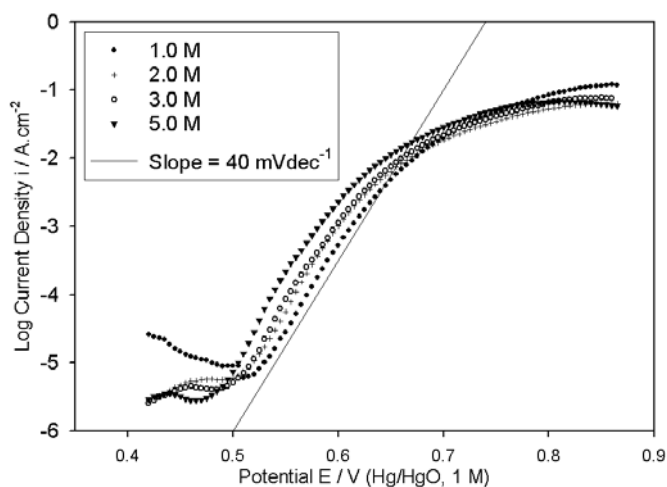


**Figure 11.**  $iR$  corrected steady state polarisation curves recorded in the direction of increasing potential for a “type” C Ni electrode in NaOH solutions of various concentration.

A reaction order plot constructed from the data of Fig. 11 at 0.550 V, in the  $\sim 40 \text{ mVdec}^{-1}$  Tafel region is presented in Fig. 12. Again the indication is that,  $m_{\text{OH}^-}$  is, as in the case of the “type” B Ni electrodes, of the order of unity.

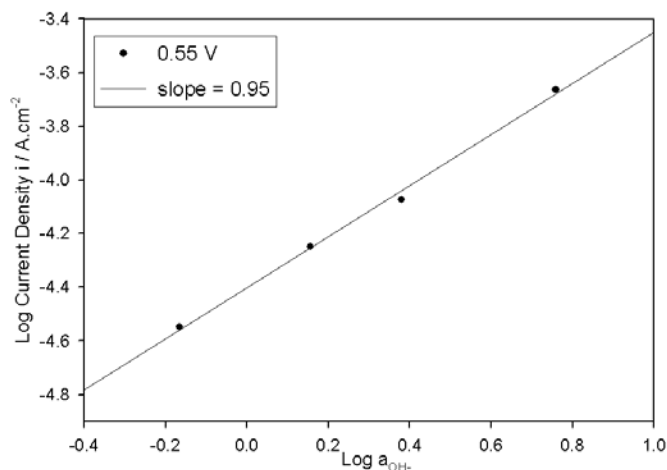


**Figure 12.** Reaction order plot based upon the polarisation curves of Fig. 11 at a potential of 0.55 V in the  $40 \text{ mVdec}^{-1}$  Tafel slope region.

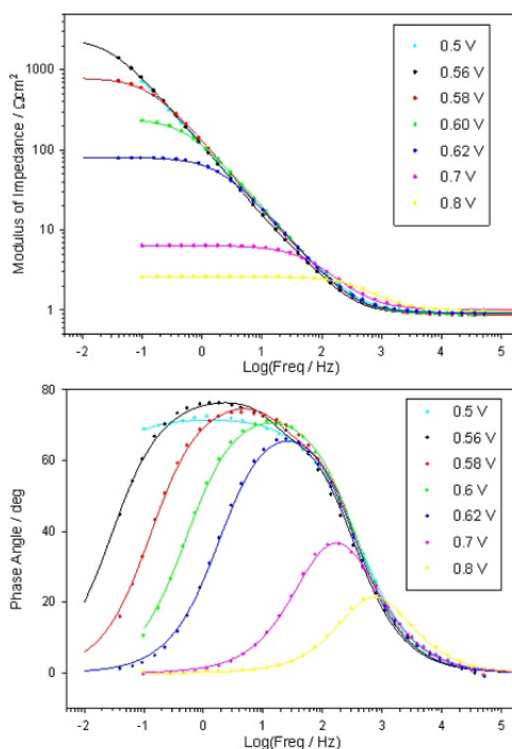


**Figure 13.** Bode plots recorded at various potentials within the region of significant OER current density for a “type” B Ni electrode in 1.0 M NaOH. Raw data are represented by circles – the continuous lines are the results of CNLS fits to the equivalent circuit model of Fig. 17.

### 3.5. Electrochemical Impedance Spectroscopy (EIS) measurements

A series of impedance spectra, recorded successively in the direction of increasing potential for a “type” B Ni electrode in 1.0 M NaOH solution are presented in the Bode representation in Fig. 13 or, equivalently, in the Nyquist (complex plane) representation in Fig. 14. Similarly, EIS data, recorded in 1.0 M NaOH at potentials associated with significant OER current densities, are presented for a “type” C Ni electrode in both the Bode and Nyquist representations in Figs. 15 and 16 respectively.

A discussion on the significance of the impedance responses of passive oxide covered Ni, Co and Fe anodes in the oxygen evolution potential region and the appropriate choice of equivalent circuit model will be presented elsewhere [44] – in this article we restrict our discussion to aspects of the EIS data related to the kinetics of the OER and to roughness factor determination. Using a CNLS fitting algorithm the raw impedance data was fitted to the equivalent circuit model depicted in Fig. 17. This model is often called the *Armstrong-Henderson equivalent circuit* [45] and has been used in the analysis of oxygen evolution for several different systems, including Pt in 1.0 M NaOH [46], Co oxide electrodeposited on Ni and Pt disk electrodes in 1.0 M NaOH [47], and Co and Ni mixed oxides on a Ni substrate also in 1M NaOH [48].

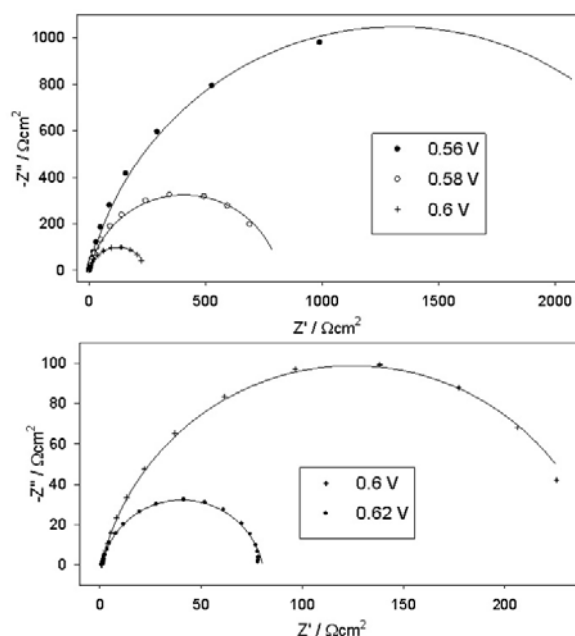


**Figure 14.** Nyquist representations of the impedance data of Fig. 13. As before, the raw data are represented by circles, while the continuous lines are the results of CNLS fits to the equivalent circuit model of Fig. 17.

The  $C_{dl}$  circuit element models the double layer capacitance, while  $R_{\Omega}$  represents the uncompensated solution resistance. The resistive elements  $R_p$  and  $R_s$  are related to the kinetics of the interfacial charge transfer reaction. Their exact significance has been discussed by Harrington and

Conway [49], who have rejected a common interpretation that  $R_p$  is the charge transfer resistance of the electroadsorption step, while  $R_s$  is the charge transfer resistance of the electrodesorption process, asserting instead that these resistive elements are the properties of two or more steps in the overall reaction. The same authors have defined  $C_\theta$  as the value of a capacitor, which in parallel with the resistance,  $R_s$ , in an equivalent circuit model, correctly models the relaxation of the charge associated with the adsorbed intermediate. They have explained that in general there is no simple relationship between this quantity and the well known *steady-state adsorption pseudocapacitance* which was discussed by Conway and Gileadi [50].

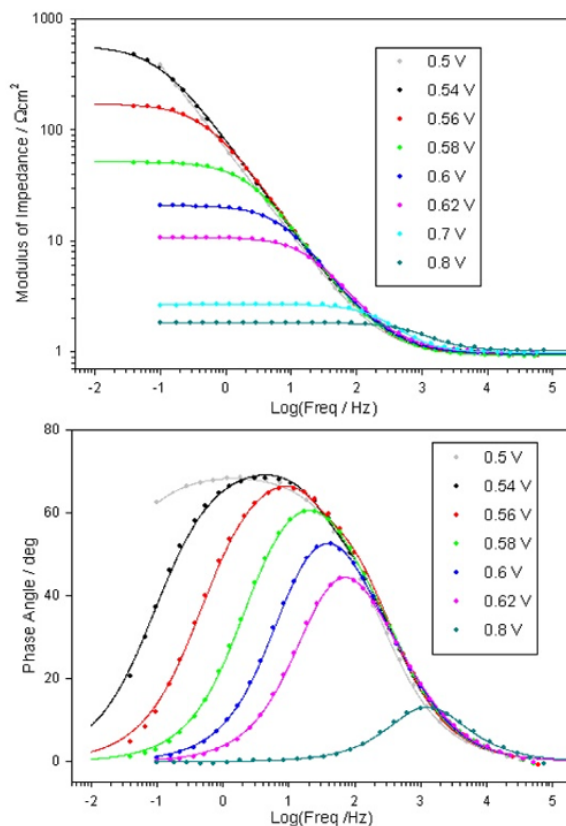


**Figure 15.** Bode plots recorded at various potentials within the region of significant OER current density for a “type” C Ni electrode in 1.0 M NaOH solution.

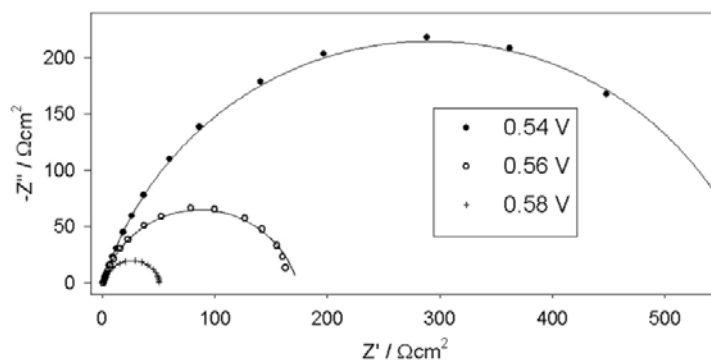


**Figure 16.** Nyquist representations of the some of the impedance data of Fig. 15.

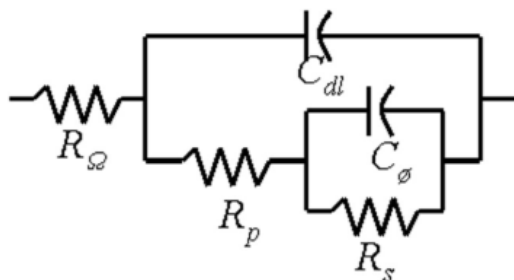


**Figure 17.** Equivalent circuit model used in the CNLS fitting of the impedance data of Figs. 13 – 16.

As is often the case, when fitting real EIS data to equivalent circuit models, it has been necessary to admit *constant phase elements* (CPEs) in place of pure capacitive elements in the equivalent circuit model of Fig. 17. This arises due to frequency dispersion in the capacitive response of the electrochemical system. For impedance data plotted in the complex plane, this frequency dispersion causes a depression of the ideal semicircular complex plane behaviour of a parallel RC combination, effectively rotating it in a clockwise direction by an angle of  $90^\circ(1-\alpha)$ , so that the centre of the semicircle no longer resides on the  $Z'$  axis, but rather below it. CPEs deal with the deviation from ideal capacitive behaviour, in an empirical manner, by expressing the impedance  $Z_{CPE}$  of a capacitive process displaying frequency dispersion as:

$$Z_{CPE} = A(j\omega)^{-\alpha} \quad (2)$$

In eqn. (2),  $A = 1/C_{\alpha=1}$ , where  $C_{\alpha=1}$  is the value of the capacitance in the absence of frequency dispersion, and  $\alpha$  is an exponent ( $\alpha \leq 1$  for a physically reasonable situation) equal to unity in the case of an ideal capacitor. CNLS fitting procedures generally return values for  $C_{\alpha=1}$  and  $\alpha$ , when asked to fit impedance data to a CPE.

The best-fit values of the equivalent circuit elements are listed in Tables 1 and 2 for the “type” B and C Ni electrodes respectively. Graphically the results of the fitting are depicted in Figs. 13 – 16 as continuous lines.

Tafel slopes are normally measured directly using dc steady state polarisation methods, however they can also be determined using impedance measurements. The latter method involves the experimental determination of the total Faradaic resistance,  $R_F$ , where in the present case,  $R_F = R_s + R_p$ . Recall that at an overpotential  $\eta$ , where simple Tafel behaviour prevails, the current density  $i$  is related to  $\eta$  via the following expression:

$$i = i_0 \exp \left[ 2.303 \frac{\eta}{b} \right] \quad (3)$$

Differentiating with respect to  $\eta$  leaves:

$$\frac{di}{d\eta} = 2.303 \frac{i_0}{b} \exp \left[ 2.303 \frac{\eta}{b} \right] \quad (4)$$

Taking the logarithm of equation (4), and noting that  $\frac{di}{d\eta} = \frac{1}{R_F}$ , where  $R_F$  denotes the Faradaic resistance, the following expression is achieved:

$$\log\left(\frac{1}{R_F}\right) = \frac{\eta}{b} + \log\left(2.303\frac{i_0}{b}\right) \quad (5)$$

implying that the inverse slope of a plot of  $\log(1/R_F)$  against  $\eta$  is equal to the Tafel slope.

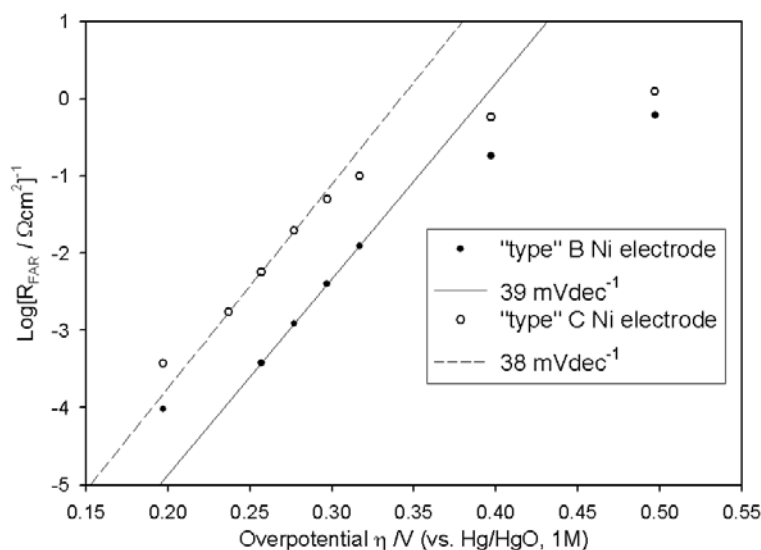


**Figure 18.**  $\log(1/R_F)$  vs.  $\eta$  plots constructed from the impedance data of Figs. 13 (“type” B) and 15. (“type” C).

Plots of  $\log(1/R_F)$  against  $\eta$  based on the listed fitting parameters of Tables 1 and 2 for Ni electrodes “types” B and C respectively, are presented in Fig. 18. It is obvious that there is excellent agreement between the Tafel slopes measured by the dc polarisation technique (Figs. 9 and 11 for “type” B and C Ni anodes respectively) and those derived from EIS measurements, with Tafel slopes of  $b \approx 40 \text{ mVdec}^{-1}$  obtained by each method at lower overpotentials.

### 3.6. Mechanistic pathways for oxygen evolution

In view of the experimental kinetic parameters outlined above, the task of mechanistic determination for the OER on Ni electrodes in aqueous alkaline media is essentially reduced to a matter of identifying an appropriate pathway with a particular rate determining step, the kinetic analysis of which will predict  $b = \frac{d\eta}{d \log i} = 2.303(2RT/3F)$  which yields a numerical value of 39.4 mV/dec at 298 K, and  $m_{OH^-} = 1$ .

**Table 1.** Optimum fit parameters for the CNLS fitting of the data of figure 13 ('type'B Ni electrode).

E	$R_s$	$C_o$	$\alpha$	$R_p$	$C_{dl}$	$\alpha$	$R_\Omega$
V	$\Omega\text{cm}^2$	$\mu\text{Fcm}^{-2}$		$\Omega\text{cm}^2$	$\mu\text{Fcm}^{-2}$		$\Omega\text{cm}^2$
0.56	2464.00	82.94	0.919	26.416	467.69	0.860	0.879
0.58	780.00	81.25	0.906	18.256	414.88	0.867	0.874
0.60	234.40	67.31	0.947	11.029	387.37	0.860	0.877
0.62	75.30	82.56	0.895	4.272	377.19	0.864	0.905
0.70	4.88	74.94	0.819	0.503	267.38	0.845	0.993

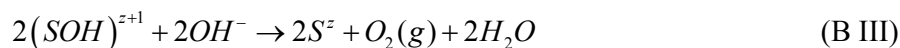
**Table 2.** Optimum fit parameters for the CNLS fitting of the data of figure 15 ('type'C Ni electrode).

E	$R_s$	$C_o$	$\alpha$	$R_p$	$C_{dl}$	$\alpha$	$R_\Omega$
V	$\Omega\text{cm}^2$	$\mu\text{Fcm}^{-2}$		$\Omega\text{cm}^2$	$\mu\text{Fcm}^{-2}$		$\Omega\text{cm}^2$
0.54	562.24	144.19	0.974	18.912	444.37	0.802	0.957
0.56	158.94	168.68	0.982	12.949	433.06	0.815	0.944
0.58	42.51	197.44	0.981	8.366	438.62	0.827	0.928
0.60	16.67	214.31	0.892	3.306	391.81	0.852	0.962
0.62	8.01	211.25	0.842	1.862	346.50	0.874	0.986

A low Tafel slope of  $2.303(2RT/3F)$  is indicative of a rate-determining step *subsequent* (although not necessarily immediately subsequent) to the initial electron transfer step. This initial step, which for virtually all proposed pathways involves the primary discharge of a single  $\text{OH}^-$  ion at each catalytically active surface site S, is characterised by a Tafel slope of  $2.303(2RT/F)$  (under Langmuir adsorption conditions - c.f. ref. 15 Table II). If it is assumed that the fractional coverage of the reaction intermediate,  $\theta$ , follows the low coverage Langmuir adsorption isotherm at lower overpotentials (i.e.  $\theta \rightarrow 0$ ), a reaction order of 1 implies that only one mole of  $\text{OH}^-$  ions from solution has been adsorbed per mole of active sites S, during the RDS or any steps preceding it. Considering earlier mechanistic analyses of the oxygen evolution reaction, it appears that only two general schemes can suitably account for our experimental kinetic parameters. The first of these is due to O'Grady and Yeager [51] or a development of the same mechanism by Burke and co-workers [52, 53]. This type of mechanism involves Ni(IV) intermediate species. The other was originally proposed by Bockris and Otagawa [15] and involves only Ni(III) reaction intermediates. While the Krasil'shchikov pathway can account for a Tafel slope of  $2.303 \times 2RT/3F$ , if the third step is considered rate controlling under Langmuir adsorption conditions with  $\theta \rightarrow 0$ , it cannot account for an associated reaction order of unity, instead giving rise to a prediction of 2 for this parameter.

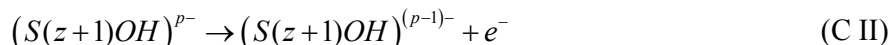
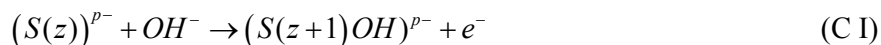
## 3.7. The Ni(IV) intermediate pathway

The pathway of O'Grady and Yeager, originally formulated to explain OER polarisation data obtained on RuO<sub>2</sub> electrodes in alkaline solution [51], is presented below:



In pathway B,  $z$  is the oxidation state of the metal ion of the electrocatalytically active surface site  $S$ . The suggestion is, that a complex species  $(SOH)^z$  is formed by the initial discharge of an  $OH^-$  ion at a metal ion site  $S^z$  – this electron is transferred directly to the external circuit, with the oxidation state of the central metal ion remaining unchanged. In the second step this metal ion is oxidised from  $S^z$  to  $S^{z+1}$  with transfer of a further electron, without discharge of a second  $OH^-$  ion.

In Burke's publications on the OER at RuO<sub>x</sub> [52] and oxidised Rh [53] electrode surfaces, the first two steps of the pathway can be generally represented as:



where,  $(S(z))^{p-}$  represents a complex hydrous oxide catalytic site with a central metal ion in the  $z$  oxidation state –  $p$  is a positive integer. It is noteworthy, that in contrast to O'Grady and Yeager's pathway, oxidation of the central metal ion occurs in the initial discharge step of scheme (C), with the second electron transfer occurring due to a one electron discharge of the overall charge on the complex surface species. The logic of the O'Grady and Yeager, or Burke et al. mechanisms is that oxygen evolution occurs to effectively “quench” an unstable higher oxide entity. A pathway, based upon the concepts of Burke et al. [52, 53], is now outlined for the case of the OER on Ni electrodes in aqueous alkaline solution.

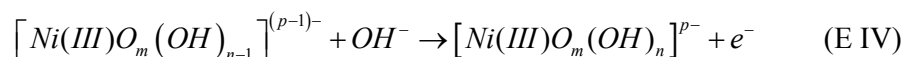
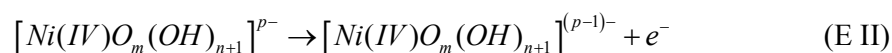
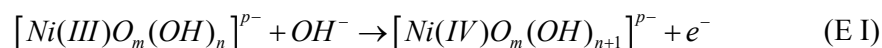
Recall from the earlier discussion regarding the complex electrochemistry of the oxidation of Ni(II) species to higher oxidation states, that the highest stable whole-number oxidation state is Ni(III). In any case this is the valance state associated with  $\beta$ -NiOOH, allegedly the “right type of oxide” for the OER [3]. In consideration of this, we believe that one view of a feasible pathway for oxygen evolution on Ni is as follows:



For mechanism (D), the unstable higher oxide that precipitates oxygen evolution (or, looking at the situation from a different angle, the OER reaction intermediate) is envisaged as being the Ni(IV)O(OH)<sub>2</sub> species.

The nature of the surface electrochemistry of hydrous oxide films, formed in aqueous solution, on electrodes of various transition metals, has been widely investigated by Burke and co-workers and was jointly reviewed by one of the present authors [54]. A common theme observed for these hydrous oxides formed is their amphoteric nature. That is to say, that these oxides act as bases (adsorbing protons or H<sup>+</sup> ions and thus acquiring positive charge) at low pH, and conversely act as acids (adsorbing OH<sup>-</sup> ions or donating protons and thus becoming negatively charged) at high pH. It is in view of the acidic nature of the hydrous oxide formed on Rh in alkaline solution, that O'Sullivan and Burke [53] envisaged that the highly charged metal ion coordinates excess hydroxide ions, and that therefore the active site for oxygen evolution can be considered as being a [RhO<sub>m</sub>(OH)<sub>n</sub>·zH<sub>2</sub>O]<sup>p-</sup> surface complex (where p=2m+n-4 for the case of Rh(IV)).

Although Burke and co-workers [52,53] made their observations regarding amphoterism, for thick hydrous oxide films formed by repetitive potential cycling, the voltammograms of Fig. 5 demonstrate that even on the first voltammetric cycle, the electrochemical properties of the passive oxide formed on nickel electrode surfaces are strongly influenced by the degree of hydration. As commented in our review on nickel hydroxide electrochemistry, the active material will never exist entirely in disordered hydrous, or in pristine anhydrous forms – in other words there will always be some degree of hydration, especially in the outer regions of the oxide film. This should certainly be true for the surface layer, in which the species catalytically active towards oxygen evolution reside. By analogy with Rh [53], and with reference to the generally accepted model of a complex non-stoichiometric higher Ni oxide discussed earlier, we suggest that the Ni(III) ions on the oxide surface at oxygen evolution potentials could reasonably be considered to be present in the form of charged complex species, that might be represented as [Ni(III)O<sub>m</sub>(OH)<sub>n</sub>]<sup>p-</sup>, where p=2m+n-3. Charge neutrality is provided by associated counterions in the outer Helmholtz layer. Taking these considerations into account, an essentially equivalent version of pathway (D) can be written, which envisages the catalytic metal ion as being complexed in an anionic surface species:



Indeed such a representation might be more correct than that presented in (D), since it would avoid the formation of the positively charged [Ni(IV)O(OH)<sub>2</sub>]<sup>+</sup> species – an entity, the existence of which runs contrary to the negatively charged surface expected for a potentially amphoteric oxide in alkaline solution. The more simplistic representation of scheme (D) is left in place, since it illustrates the fundamental nature of the reaction very clearly and follows the traditional notion of β-NiOOH

being the active material for oxygen evolution [3]. In any case, if (as is most likely)  $m = 1$ , the  $[\text{Ni(III)O}_m(\text{OH})_n]^{p-}$  species is merely a NiOOH surface group that has coordinated extra hydroxide ions, owing to the acidic nature of the hydrous oxide.

A formal kinetic analysis is now conducted, demonstrating, that if the *second step* in mechanisms (D) or (E) is considered to be rate-determining, and if low coverage ( $\theta \rightarrow 0$ ) Langmuir adsorption of the Ni(IV) reaction intermediate (formed in the respective first steps) is admitted, then the experimental kinetic parameters can be satisfactorily rationalised.

The rates of reaction for step (E1) in both the forward (defined via the flux  $f_1$  with units of  $\text{mol cm}^{-2}\text{s}^{-1}$ ), and reverse (again defined via the flux  $f_{-1}$ ) directions can be written as:

$$f_1 = k_1^0 a_{\text{OH}} (1 - \theta) \exp\left[\frac{\beta F \eta}{RT}\right] \quad (6)$$

And

$$f_{-1} = k_{-1}^0 \theta \exp\left[-\frac{(1 - \beta) F \eta}{RT}\right] \quad (7)$$

where,  $\theta$  is the fractional coverage of the electrode surface by the adsorbed species,  $[\text{Ni(IV)O}_m(\text{OH})_{n+1}]^{p-}$ ,  $k_1^0$  and  $k_{-1}^0$  are standard electrochemical rate constants, while  $\beta$  is the symmetry factor associated with the electron transfer energy barrier. Under the hypothesis of pseudo-equilibrium, we assume that  $f_1 = f_{-1}$  and thus extract the following expression for  $\theta$ :

$$\theta = \frac{K a_{\text{OH}} \exp\left[\frac{F}{RT} \eta\right]}{1 + K a_{\text{OH}} \exp\left[\frac{F}{RT} \eta\right]} \quad (8)$$

where  $K = k_1^0 / k_{-1}^0 = \exp[-\Delta G^0 / RT]$ . At lower values of  $\eta$ , the  $\Delta G^0$  term will dominate the exponent in equation (8), which will therefore be a significant negative quantity, and thus, in this overpotential range  $K a_{\text{OH}} \exp[F\eta/RT] \ll 1$ , and equation (8) reduces to:

$$\theta \cong K a_{\text{OH}} \exp\left[\frac{F \eta}{RT}\right] \quad (9)$$

Since  $\theta \cong K a_{\text{OH}} \exp[F\eta/RT] \ll 1$ , it is clear that at low overpotentials, the Langmuir isotherm is operative in its low coverage mode. The general expression for the rate equation of step (E II) is written as:

$$f_2 = k_2^0 \theta \exp\left[\frac{\beta F \eta}{RT}\right] \quad (10)$$

Since this step is envisaged to be rate determining it will also describe the rate for the overall process and so we obtain that the net reaction flux is:

$$f_{\Sigma} \cong f_2 = Kk_2^0 a_{OH} \exp\left[\frac{(1+\beta)F\eta}{RT}\right] \quad (11)$$

The transfer rate of two electrons is limited by the velocity of the RDS – therefore the overall current density for oxygen evolution can be written as:

$$i = 2Ff_{\Sigma} = 2Fk_2^0 a_{OH} \exp\left[\frac{(1+\beta)F\eta}{RT}\right] \quad (12)$$

Assuming a symmetrical electron transfer energy barrier for step (E II) (i.e.  $\beta = 1/2$ ), it can readily be shown from equation (12), that the following values arise for the Tafel slope,  $b$ , and the reaction order with respect to  $OH^-$  ion activity,  $m_{OH^-}$ :

$$b = \left(\frac{\partial \eta}{\partial \log i}\right)_{a_{OH}} = 2.303 \left(\frac{2RT}{3F}\right) \quad (13)$$

$$m_{OH^-} = \left(\frac{\partial \ln i}{\partial \ln a_{OH^-}}\right)_{\eta} = 1 \quad (14)$$

Hence, it is apparent that the mechanistic pathways outlined in schemes (D) or (E), can predict the experimental parameters of  $b = \sim 40 \text{ mVdec}^{-1}$ , and  $m_{OH^-} = \sim 1$ .

The kinetic analysis for the pathway of O'Grady and Yeager, with step (B II) considered to be the RDS, is formally identical to that presented in equations (6) to (14). Indeed, by analogy to mechanism (B), steps (E III) and (E IV) of our proposed pathway could be replaced by the following alternative step:

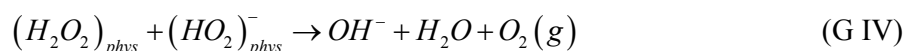
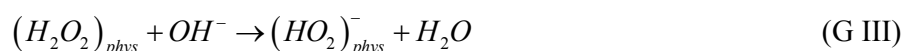
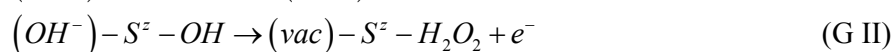
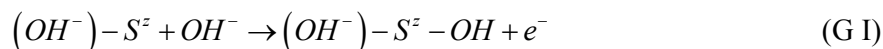


However, it is intuitively rather difficult to understand how step (F), which requires the interaction of two surface species, could proceed at any appreciable rate under the required low coverage Langmuir conditions. The steps proposed by Burke et al. [52, 53] subsequent to the RDS, would seem to be more realistic, and this is a major factor in our adoption of the type of pathway envisaged by these workers, in preference to pathway (B). It is worth noting that a stoichiometric number of  $\nu = 2$  is associated with a rate-determining second step in mechanism (B), as opposed to a value of  $\nu = 1$  for a rate-limiting second step in schemes (D) or (E). If the stoichiometric number could

be accurately experimentally determined, it would be possible to confidently admit one of these types of mechanistic pathway, while dismissing the other. However, the extreme irreversibility of the oxygen evolution and reduction processes, means that practical experimental kinetic studies on the respective reactions must be conducted at widely separated potentials. As a result of this, it is inevitable that the electrode surface differs considerably at the experimental potential windows of the reduction and evolution reactions, and hence the anodic and cathodic processes are not complementary. It is therefore widely believed that the principle of microscopic reversibility cannot be applied to the oxygen electrode, and consequently experimentally determined values of the stoichiometric number are unreliable [9].

### 3.8. The Ni(III) intermediate pathway

Amongst the conventionally listed candidate pathways for the OER (e.g. see refs. 2, 15 Table II or 55), only mechanisms like paths (B) or (E), involving the formation of a higher valance state of the metal ion, can account for the experimental kinetic parameters of  $b = \sim 2.303 \times 2RT/3F$  accompanied by  $m_{OH^-} = \sim 1$ . The aforementioned “conventional pathways” assume that all the O atoms of the evolved  $O_2$  gas originate from solution phase  $OH^-$  ions. In contrast to this, Bockris and Otagawa [15] devised the following mechanism for oxygen evolution at  $LaNiO_3$  electrodes in aqueous alkaline solution:

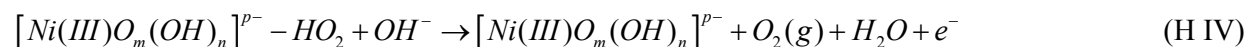
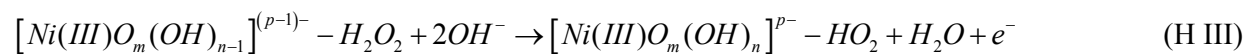
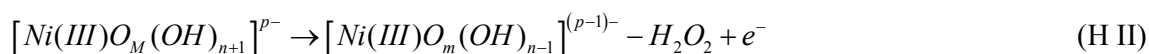


Pathway (G) is special case of the more general *physisorbed peroxide mechanism* proposed by the same authors for the OER at electrodes of the wider perovskite family [15]. We have proposed elsewhere [56] that this more general peroxide pathway is the operative OER mechanism at multi-cycled Fe electrodes in alkaline solution, and have treated this type of reaction path in some detail therein. In pathway (G), (vac) denotes an oxygen vacancy at the surface of the  $LaNiO_3$  lattice, while  $(OH^-)$  represents an  $OH^-$  ion in the surface occupying the vacancy site. The  $(OH^-) - S^z$  reaction site is envisaged to be originally formed through the acceptance of a proton by an oxide surface  $O^{2-}$  ion from  $H_2O$ . Significantly, this means that *oxygen atoms from the oxide surface are postulated to partake directly* in the gas evolution reaction. Bockris and Otagawa [15] obtained the same values of  $b$  and  $m_{OH^-}$  for the OER at their nickelate anode as were observed for passive oxide covered Ni electrodes in the present study. They showed that these parameters can be rationalised, *without the need for oxidation of the metal ion* of the reactive site, by admitting pathway (G) with the second step as the RDS. In mechanism (G), the metal cations of the catalytically active sites play a more “passive” role than in mechanisms (B) or (E), facilitating the coordination of an OH group in the primary discharge

step, without actually being oxidised to a higher valance state. For the former mechanism, the electrode effectively acts as an electron sink, facilitating the transfer of electrons from OH<sup>-</sup> ions to the external circuit, but with no oxidation of metal cations.

The formal kinetic analysis adopted by Bockris and Otagawa [15] is similar to that presented in equations (6) to (14), except that an additional term,  $\theta_V$ , must be factored in, by comparison to equation (10) (and thus (11) and (12)), to account for the coverage of OH<sup>-</sup> ions in the lattice. Bockris and Otagawa assumed that  $\theta_V$  was invariant with potential, having an intermediate value and was therefore significantly greater than  $\theta$ , which was assumed to be very small (low coverage Langmuir adsorption isotherm). Owing to the lack of dependance of  $\theta_V$  on  $\eta$  or  $a_{OH}$ , the final result of the kinetic analysis is identical to equations (13) and (14) [15].

The question of whether oxygen atoms from the oxide surface can participate directly in the OER is the subject of considerable controversy [57], and probably for this reason, pathways based upon this concept have been slow to gain widespread acceptance in the literature. However, if we adopt the ideas of Burke et al., as discussed in the previous section, regarding the acidic nature of hydrous oxide surfaces at significant anodic potentials in solutions of high pH, it is possible to write a scheme similar to (G), that does not require the possibly dubious admission of direct participation of surface oxygen species in the OER. For the case of anodic oxide covered Ni anodes such a pathway might be written as follows:



In step (H II), the electron lost to the external circuit is provided by an excess coordinated OH<sup>-</sup> ion, leading to an overall decrease of one in the net negative charge of the surface complex. We have chosen to alter the pathway of Bockris and Otagawa [15<sup>1</sup>] (scheme G) in the steps following the RDS (H II), for the same reason that we expressed a preference for pathway (E), as opposed to (F), namely, that it is difficult to envisage how the chemical recombination reaction in step (G IV) could proceed sufficiently rapidly, under low coverage Langmuir adsorption conditions, such as not to render it rate determining. Of course in essence, the concepts of surface anionic complexes, on one hand, and OH<sup>-</sup> ions occupying surface oxygen vacancies on the other, are actually different ways of approaching the same phenomenon – the anionic character of oxides in aqueous alkaline solution. However, given the controversy regarding the direct participation of lattice oxygen atoms in the OER, the anionic complex representation of pathway (H), may well be a more widely acceptable representation of this type of oxygen evolution mechanism than the surface vacancy model of pathway (G). The formal kinetic analysis of scheme (H) is of course identical to that of scheme (G), as dicussed above and therefore pathway (H) suitably accounts for the experimental values of  $b$  and  $m_{OH^-}$ .

### 3.9. The relative merits of the Ni(III) and Ni(IV) intermediate pathways

Although our electrochemical measurements have, by our reckoning, lead to the suggestion of two candidate mechanisms (effectively (D)/(E) or (H)) to the exclusion of all other proposed pathways, these measurements cannot further discriminate between the two.

The Ni(IV) intermediate mechanism of scheme (D)/(E) will appeal to the school of thought that envisages the OER to be essentially a “side reaction” facilitating the decomposition of unstable higher oxide entities. Furthermore when written as scheme (D) there is no need for the introduction of hypothetical representations of the anionic nature of the oxide surface in alkaline solution.

One of the major advantages of the Ni(III) intermediate mechanism of scheme (H) is that it can account satisfactorily for the loss of oxygen evolution activity with time, that was observed and discussed by Lu and Srinivasan [3]. Quite reasonably, these authors attributed this behaviour to an increase in the relative proportion of  $\text{Ni}^{4+}$  compared to  $\text{Ni}^{3+}$  surface ions, envisaged to occur by the oxidation, upon extended polarisation, of the catalytically active  $\beta\text{-NiOOH}$  to  $\text{NiO}_2$ . However, their proposed reaction mechanism, a modified Krasil'shchikov scheme, also proposed that  $\text{NiO}_2$  partakes in the OER as a transient reaction intermediate. It is rather difficult to rationalise how the Ni(IV) species can present an inert surface site for the OER, yet act as an intermediate for the same reaction. This difficulty is removed by our pathway (H) which doesn't require a Ni(IV) intermediate.

In addition to this, it will be shown in the second and third installments of this series of papers, that the experimental kinetic parameters for the OER at passive oxide covered Co and Fe electrodes are not suggestive of a mechanism involving the “quenching” of an unstable higher oxide species, implying that this concept cannot be taken as a general rule for the reaction. Furthermore, as will be discussed in the third installment, if we seek to understand the relative OER catalytic performances of anodic oxide covered Fe, Co and Ni electrodes in terms of a coherent theory of electrocatalysis, it is necessary that the RDS for the reaction at the Ni anode should involve the desorption of an OH entity. This criterion is clearly satisfied by mechanism (H) but not by mechanism (D)/(E).

In view of the discussion of the preceding two paragraphs, it is our view that the Ni(III) intermediate pathway, (H), is more likely than the Ni(IV) intermediate route, (D)/(E), to be the operative OER mechanism at passive oxide covered Ni anodes in aqueous alkaline solution.

As a final remark on the reaction mechanism, it was noted in the introduction, that a study of the variation of OER catalytic activity with  $\text{OH}^-$  activity was also performed for Ni electrodes by Bronoel and Reby [10]. After an in-depth discussion these workers proposed the Krasil'shchikov mechanism, as presented in scheme (A), to be the most likely reaction pathway. Despite raising some interesting points, their mechanistic designation is however inconsistent with their experimental data. For example, in steady state polarisation measurements a transfer coefficient of  $\alpha = \sim 1.2$  was reported at lower values of  $\eta$ . Since  $b = 2.303 \times RT/\alpha F$ , this corresponds to  $b \approx 2.303 \times 4RT/5F$ . It was proposed by Bronoel and Reby that the rate of the OER at these overpotentials was determined by the initial  $\text{OH}^-$  discharge step - i.e. (A I). However as was discussed previously, rate control by this step is always characterised by  $b \approx 2.303 \times 2RT/F$  - we cannot therefore concur with the conclusions of Bronoel and Reby [10].

### 3.10. Electrode roughness factor measurements – theoretical considerations

In order to make a meaningful comparison between the OER electrocatalytic activities of the three “types” of Ni electrode, and indeed between the catalytic performance of these anodes and electrodes of other materials, it is necessary to obtain values of the electrode roughness factor,  $f_r$ , for each electrode. Although a critical appraisal of 15 methods for electrode real surface area determination has been provided [58], few or none of these techniques are useful for the quantification of the specific surface area available to the OER, on passive oxide covered Ni electrodes. In view of this, we’ve had to turn to a rather novel in-situ method, pioneered by Ho and Piron [26, 27], the experimental details of which, have already been discussed. While the reader should refer to the original works of Ho and Piron for an in-depth discussion of the technique and the assumptions on which it is based, a very brief treatment essential to the understanding of our data is presented here.

Essentially the technique is based on the assumption that the measured quantity,  $Q_{dec}$ , is the charge passed in the desorption of the intermediate species involved in the OER. In the case of scheme (H), our preferred OER pathway, the only intermediate species envisaged to occur with a significant fractional coverage,  $\theta$ , is the  $[Ni(III)O_m(OH)_{n+1}]^{p-}$  formed in the first step. Therefore, when the anodic charging current  $i_{appl}$  is interrupted, the discharge of the electrode can occur via the following overall reaction, which we propose to give rise to the cathodic transients recorded on the oscilloscope-



This reaction is consistent with the prediction of Conway and Bourgault [4] that the self discharge of a nickel hydroxide electrode should continue until the nickel ions are in the Ni(II) valance state, since the reversible potential of the Ni(II)↔Ni(III) redox transition is anodic to the oxygen electrode reversible potential. Incidentally, at the lower potentials associated with Ni(II) species, the coordination of excess OH<sup>-</sup> ions by surface metal cations is less likely and so p on the right hand side of (15) is probably equal to zero. The formula, p=2m+n-3, is then satisfied by m = 1 and n = 1 and so the discharged species is Ni(OH)<sub>2</sub>, in accord with the Bode scheme (Fig. 2).

As was also reported by Ho and Piron [27], upon plotting  $Q_{dec}$  vs.  $\eta$  ( $\eta$  is of course related to the experimental variable  $i_{appl}$  through the steady state polarisation curve for a given electrode), it was noted that  $Q_{dec}$  increased with  $\eta$ , for the lower values of the latter, associated with the lower Tafel slope region in the steady state polarisation curve for the same electrode – see for example the data related to the “type” A Ni electrode in Fig. 20. At higher overpotentials, plateau regions were observed in the  $Q_{dec}$  vs.  $\eta$  plots. Ho and Piron proposed that the relatively constant  $Q_{dec}$  values associated with this plateau region corresponds to the desorption of OH<sub>ads</sub> for the situation where the fractional coverage  $\theta$  of this intermediate tends towards unity. Based upon theoretical considerations of Fedorova and Frumkin<sup>59</sup>, it was assumed by Ho and Piron<sup>27</sup>, that the charge passed during the two electron desorption (via a reaction like that of equation (15)) of a monolayer of OER intermediate species could be taken as 420  $\mu Ccm^{-2}$ . On this basis the roughness factor for OER anodes can be *estimated* using the following expression:

$$f_r = \frac{Q_{dec}(plateau)}{420 \mu C cm^{-2}} \quad (16)$$

We use the word “estimated” as opposed to “evaluated” above, because as pointed out by the pioneers of the technique [27], the benchmark value of  $420 \mu C cm^{-2}$ , merely serves as a reasonable “universal accepted standard”, while in reality the exact charge passed during the desorption of a full monolayer of reaction intermediates is uncertain. It is therefore emphasised at this point, that we are fully aware of the weaknesses of the  $OH_{ads}$  desorption method. However it is not our aim to obtain absolute values of the true surface areas of the electrodes, but rather to obtain estimates of roughness factors, in order to facilitate a more meaningful comparison of the intrinsic catalytic activities of the different “types” of Ni anode towards the oxygen evolution reaction. The same technique was applied to roughness factor estimation for Co and Fe electrodes, allowing us to perform, in the third part of this series, a truly significant comparison of the relative OER activities of passive oxide covered electrodes of the three metals.

### 3.11. Electrode roughness factor measurements – results

Several raw discharge current vs. time transients, recorded using the apparatus of Fig. 1, for a “type A” Ni electrode in 1.0 M NaOH, are presented in Fig. 19. The overall results of the current decay experiments for this system, and for “type” B and C Ni anodes, also in 1 M NaOH, are presented in Fig. 20. The  $i_{appl}$  values for the “type” B and C electrodes were of course derived from steady state polarisation data for those particular systems – in Fig. 20, to maintain clarity, only the polarisation curve for a “type” A electrode has been included. The  $Q_{dec}(\eta)$  data points represent the mean value of  $Q_{dec}$  calculated from the four transients recorded for each value of  $i_{appl}$ , while the vertical error bars span  $\pm$  one standard deviation from this mean.

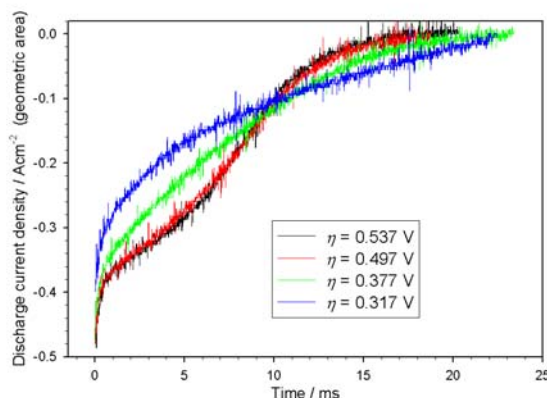


**Figure 19.** Raw decay current transients for a “type” A Ni electrode in 1.0 M NaOH solution. Indicated are the overpotentials corresponding to the values of  $i_{appl}$  in each case.

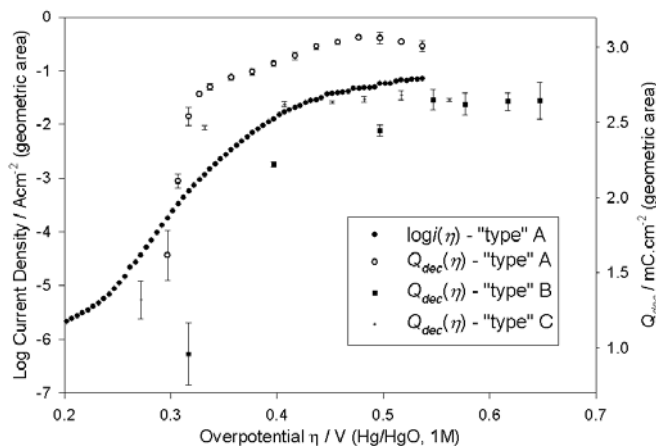


**Figure 20.** Total charge,  $Q_{dec}$ , passed during the discharge of the various “types” of Ni electrode in 1.0 M NaOH vs. oxygen evolution overpotential  $\eta$ . Also included is the steady state polarisation curve for the “type” A electrode.

As expected, there is a close relationship between the OER steady state polarisation curve and the  $Q_{dec}(\eta)$  plot presented for the “type” A anode in Fig. 20. For this particular system, the values of  $Q_{dec}$  are approximately constant (i.e. lie in the range from approximately 3.0 – 3.1 mCcm<sup>-2</sup>) over a range of  $\eta$  from 0.437 – 0.517 V – this would appear to be the  $\theta \approx 1$  plateau region as was observed by Ho and Piron<sup>27</sup> for their electrodeposited Ni, Co and Ni<sub>20</sub>Co<sub>80</sub> electrodes. The magnitude of  $Q_{dec}$  decreases gradually with decreasing overpotential for  $\eta < 0.437$  V, before dropping dramatically for  $\eta \leq 0.317$  V - i.e. in the lower Tafel slope region of potential, where it was envisaged in our kinetic analysis, that  $\theta \rightarrow 0$ .

Taking the mean of the  $Q_{dec}$  values over the range of overpotentials from 0.457 – 0.517 V, yields 3.047 mCcm<sup>-2</sup>. A reasonable estimate of the experimental error is the difference between this mean value and that value of  $Q_{dec}$ , covered by the error bars of the data points for  $0.457 \geq \eta \geq 0.517$  V, which is furthest from the mean – performing such an analysis yields an estimate for  $Q_{dec}(\text{plateau})$  of  $3.05 \pm 0.05$  mCcm<sup>-2</sup>. Inserting this value into equation (16) yields an estimate of the roughness factor for the fresh non-pre-treated Ni electrode of  $f_r = 7.3 \pm 0.1$ . The quoted error is of course, merely the experimental error – in reality the true error is likely to be much larger owing, as was outlined in the previous section, to the questionable nature of some of the assumptions on which the technique is based [27]. A similar analytical technique was used to evaluate the values of  $f_r$  for the “type” B and C electrodes, and the results are summarised in Table 3.

Another well known approach in the estimation of electrode roughness factors is the so-called *double layer capacitance ratio* method [58]. Briefly, this method is based on the fact, that if a reference value were available for the double layer capacitance per unit area of an ideally smooth electrode surface, then the roughness factor of a given electrode could be estimated by dividing its experimentally determined  $C_{dl}$  value by this reference value. The capacitance ratio method was used by Ho and Piron [27], to provide a comparison for real surface area values, which they determined by the

OH<sub>ads</sub> desorption method. Following an earlier work by Frumkin [60], they adopted the value of 40  $\mu\text{Fcm}^{-2}$  as the double-layer capacitance for a smooth, oxide covered electrode. As with the OH<sub>ads</sub> desorption method, uncertainty about the reference value is one of the major drawbacks of the double layer capacitance ratio approach.

**Table 3.** Summary of the roughness factors,  $f_r$ , determined for the various “types” of Ni electrode in 1.0 M NaOH solution, using the OH<sub>ads</sub> desorption method.

Ni Electrode “type”	$Q_{dec}(\text{plateau})$ $\text{mCcm}^{-2}$	$f_r$
A	$3.05 \pm 0.05$	$7.3 \pm 0.1$
B	$2.64 \pm 0.09$	$6.3 \pm 0.2$
C	$2.68 \pm 0.03$	$6.4 \pm 0.1$

Since we had already recorded EIS spectra for “type” B and C Ni electrodes in 1.0 M NaOH solution (see Figs. 13 – 16) and obtained CNLS fitting values for the double layer capacitance of these electrodes (Tables 1 and 2), it was decided to compare the values of  $f_r$  yielded by the double layer capacitance ratio method, with those estimated by the OH<sub>ads</sub> desorption technique. To maintain consistency with Ho and Piron [27], 40  $\mu\text{Fcm}^{-2}$  was adopted as the ‘benchmark’ double-layer capacitance for a smooth oxide covered electrode – it is however noteworthy that Bockris and Otagawa [61] choose a reference value of  $C_{dl} = 60 \mu\text{Fcm}^{-2}$  for the estimation of roughness factors for perovskite electrodes in 1 M NaOH. The CNLS values of Tables 1 and 2 refer to a double layer CPE, as opposed to a pure capacitance – a method proposed by Jovic [62] was used to calculate an effective value of the double layer capacitance,  $C_{dl\text{ eff}}$ , from the fitted CPE ( $C_{\alpha=1}$ ,  $\alpha$ ) and  $R_p$  parameters.

Values of  $C_{dl\text{ eff}}$  and  $f_r$  are listed in Tables 4 (“type” B electrode) and 5 (“type” C) for the various overpotentials at which CNLS fitting was applied to raw EIS data. It is apparent that the values of  $C_{dl\text{ eff}}$  and consequently the estimates of  $f_r$  decrease steadily with increasing  $\eta$ . This trend is probably due to a decrease in the electrode surface area in physical contact with electrolyte solution – it is after all this “wetable” surface area that is sensitive to determination by the double layer capacitance ratio method. The effect is most likely caused by vigorous oxygen bubble formation at higher OER overpotentials<sup>63</sup>. The “wetable” surface area may be somewhat diminished by the momentary adhesion of gas bubbles to the oxide surface at some of the catalytic reaction sites – an effect that would lead to a time-averaged apparent decrease in surface area over the course of the periods of imposition of the EIS perturbation signal at a given frequency. However these sites are still available for the OER – in fact they are not “wetable” over the short timescale at which the double layer discharges ( $R_p C_{dl} \sim \text{ms}$  for the data of Tables 4 and 5), precisely because they are (or have just been) involved in an act of gaseous oxygen evolution.

**Table 4.** Calculated values for the effective double layer capacitance,  $C_{dl, eff}$ , of a “type” B Ni electrode in 1.0 M NaOH at various overpotentials  $\eta$ , based upon the optimised  $C_{dl}$ ,  $\alpha$  and  $R_p$  parameters of Table 1. Also included are the associated estimates of the electrode roughness factor  $f_r$ .

$E$ V	$\eta$ V	$R_p$ $\Omega\text{cm}^2$	$C_{dl}$ $\mu\text{Fcm}^{-2}$	$\alpha$	$C_{dl, eff}$ $\mu\text{Fcm}^{-2}$	$f_r$
0.56	0.257	26.416	467.69	0.860	252.50	6.3
0.58	0.277	18.256	414.88	0.867	216.73	5.4
0.60	0.297	11.029	387.37	0.860	180.65	4.5
0.62	0.317	4.272	377.19	0.864	157.25	3.9
0.70	0.397	0.503	267.38	0.845	66.85	1.7

**Table 5.** Calculated values for the effective double layer capacitance,  $C_{dl, eff}$ , of a “type” C Ni electrode in 1.0 M NaOH at various overpotentials  $\eta$ , based upon the optimised  $C_{dl}$ ,  $\alpha$  and  $R_p$  parameters of Table 2. Also included are the associated estimates of the electrode roughness factor  $f_r$ .

$E$ V	$\eta$ V	$R_p$ $\Omega\text{cm}^2$	$C_{dl}$ $\mu\text{Fcm}^{-2}$	$\alpha$	$C_{dl, eff}$ $\mu\text{Fcm}^{-2}$	$f_r$
0.54	0.237	18.912	444.37	0.802	172.39	4.3
0.56	0.257	12.949	433.06	0.815	166.40	4.2
0.58	0.277	8.366	438.62	0.827	166.50	4.2
0.60	0.297	3.306	391.81	0.852	146.43	3.7
0.62	0.317	1.862	346.50	0.874	137.29	3.4

In view of this it would seem, that the most appropriate value of  $C_{dl, eff}$  for the estimation of  $f_r$ , is that derived from EIS data recorded at overpotentials just above the onset potential for significant OER current densities. Adopting this approach, if the roughness factor estimate for the “type” B electrode is based upon the impedance data recorded at  $\eta = 0.257$  V, we have  $f_r = 6.3$ . Clearly this is in excellent agreement with the roughness factor of  $f_r = 6.3 \pm 0.2$ , determined by the transient decay method for the same electrode in the same electrolyte solution. Indeed this level of agreement between these two methods of roughness factor estimation is somewhat surprising, considering their relative crudeness as experimental approaches.

In the case of the “type” C Ni electrode there is, however, a significant disparity between the values of  $f_r$  estimated by the two methods. The  $\text{OH}_{\text{ads}}$  desorption method delivers a value of  $f_r = 6.4 \pm 0.1$  (Table 3), while by consulting Table 5, it is clear that the values of  $C_{dl, eff}$  for lower overpotentials (i.e.  $0.237 \leq \eta \leq 0.277$ ), lead to an  $f_r$  estimate of 4.2 – 4.3. The lower estimate yielded by the double layer capacitance method may arise due to the relatively low values (0.802 – 0.827, see Table 5) of the CPE  $\alpha$  parameters for  $C_{dl}$  at the overpotentials from which the  $f_r$  estimate is derived. The lower the  $\alpha$  parameter, the less identifiable is the raw impedance data with the classical concept of a capacitance. In the case of the “type” B Ni electrode, the  $\alpha$  parameter for the EIS data recorded at  $\eta = 0.257$  has a value of 0.86, implying that the impedance response in this case is more genuinely characteristic of a conventional double layer capacitance as compared to the impedance response for the “type” C Ni

electrode at this overpotential ( $\alpha = 0.815$ ). The roughness factor of 6.3, estimated, in the case of the 0.86  $\alpha$  parameter was in good agreement with that estimated from the transient decay method (“type” B electrode) – by comparison the value of  $f_r$  arising from the CNLS fitting parameters with lower  $\alpha$  values (“type” C electrode) did not agree so well with the roughness factor estimated for this electrode by the alternative method.

### 3.12. Comparison of the intrinsic activities for the OER of the differently pre-treated Ni electrodes

Steady state polarisation curves for the three “types” of Ni electrode, with the current density values normalised according to the roughness factors of Table 3, are presented in Fig. 21. The OER steady state current density for the “type” C Ni electrode at the arbitrary overpotential of 0.302 V is  $i = 1.34 (\pm 0.02) \times 10^{-4} \text{ Acm}^{-2}$ . This is over ten times greater than that ( $i = 1.21 (\pm 0.04) \times 10^{-5} \text{ Acm}^{-2}$ ) observed at the same overpotential for the “type” B electrode. An intermediate value of  $i = 3.34 (\pm 0.05) \times 10^{-5} \text{ Acm}^{-2}$  is observed for the minimally pre-treated “type” A Ni electrode at  $\eta = 0.302 \text{ V}$ .

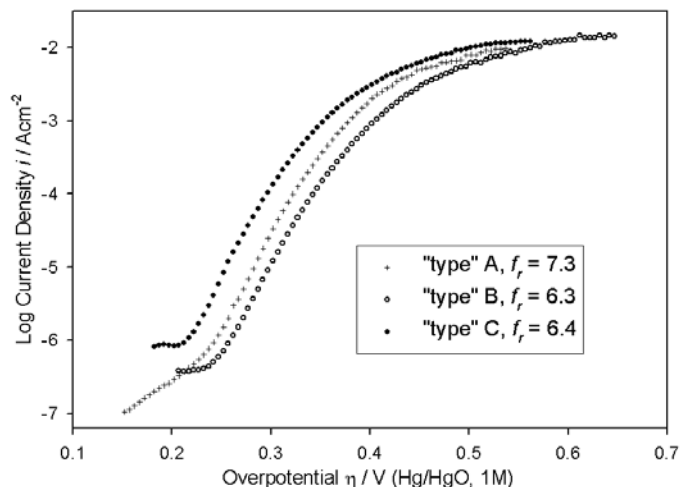


**Figure 21.**  $iR$  corrected steady state polarisation curves recorded in 1.0 M NaOH solution, for the various “types” of Ni electrode. The values of  $\log i(\eta)$  are normalised to the estimated truly active surface areas, based on the stated roughness factors.

The  $Q_{dec}$  vs.  $\eta$  plots of Fig. 20 point to similar values of  $Q_{dec}(\text{plateau})$  for these particular specimens of the “type” B and C anodes, which in turn leads to similar estimates for  $f_r$ . The key difference is that the onset potential for the  $Q_{dec}(\eta)$  “plateau” occurs in the region of  $\eta \approx 0.45 \text{ V}$  for the C “type” electrode, as compared to  $\eta \approx 0.55 \text{ V}$  for the “type” B electrode. This suggests that while the surface area available for the OER is similar for both electrodes, the pre-oxidation regime (routine C) produces an oxide surface with a *higher concentration of the more catalytically active form* of the nickel oxyhydroxide ( $\beta\text{-NiOOH}$  if the concepts of Lu and Srinivasan<sup>3</sup> are adopted) towards oxygen evolution. Therefore at lower values of  $\eta$ , discharge of  $\text{OH}^-$  ions from solution to form the OER intermediate species ( $[\text{Ni(III)O}_m(\text{OH})_{n+1}]^p$  according to step (H I)) occurs at a relatively larger

concentration of surface  $\text{Ni}^{3+}$  ions for the “type” C relative to the “type” B electrode. From Fig. 21, it would appear that once the applied overpotential reaches  $\eta \approx 0.5$  V for the former, all Ni oxide surface sites with the potential to catalyse oxygen gas evolution are active with respect to reaction (H I), and thus a limiting current density is observed in the  $\log i$  vs.  $\eta$  plot.

Owing to the less active nature of the oxide surface produced by the pre-reduction regime (routine B), a higher applied potential is necessary to achieve the same OER current density at the “type” B electrode relative to the “type” C. Across the lower overpotential region of Fig. 21, associated with parallel  $\log i$  vs.  $\eta$  plots ( $b = \sim 2.303 \times 2RT/3F \text{ mVdec}^{-1}$ ) for the three Ni electrodes, it is obvious that an applied potential, greater in magnitude by  $\sim 40$  mV, is required to achieve the same rate of reaction at the “type” B electrode as at the “type” C electrode. Since we have estimated similar values of  $f_r$  for both electrodes, this difference in overpotential might be envisaged to reflect the extra energy required to make the OER proceed with the same rate, at a surface with a lower concentration of the “right type of oxide” for the catalysis of the reaction. The extra energy is required to achieve reaction at the less optimal catalytic sites, possibly identifiable with the  $\gamma$ -Ni phase of the Bode scheme – recall Fig. 2. According to this description, given two Ni electrodes with different “levels” of activity towards the OER, the difference in applied potential required to achieve the same rate of reaction (normalised to account for real surface area) at the two electrodes, will be governed by the relative proportions of the less and more active Ni sites at each electrode surface.

In terms of the real surface area normalised data of Fig. 21, the “type C” (pre-oxidised) electrode might be considered to be that with the largest relative concentration of “more active” Ni sites. The pre-oxidation routine obviously has the effect of increasing the surface concentration of these sites relative to the minimally pre-treated, “type” A Ni electrode. In contrast the pre-reduction treatment (“type” B) has the effect of decreasing the relative proportion of these “more active” sites by comparison with the “type” A electrode.

#### 4. CONCLUSIONS

The oxygen evolution performance of passive oxide covered polycrystalline Ni anodes, depends on the history of the electrode (i.e. pre-treatment regime in the context of the present study), however the reaction mechanism, as indicated by the Tafel slope and the reaction order with respect to  $\text{OH}^-$  activity, was found to be consistent for three relatively mild electrochemical pre-treatment routines. Only two of the pathways previously proposed for the OER, were consistent with our experimental data. In the overall context of our work on oxygen evolution at electrodes of other metals, we are inclined to favour a pathway, (H), which involves intermediate species in the Ni(III) valance state only. An alternative mechanism that envisages the oxidation of the active Ni metal ion centres to the +4 oxidation state cannot be entirely dismissed. The anionic nature of the passive oxide surface, at significant anodic potentials in solutions of high pH, is likely to facilitate oxygen evolution. The admission of this concept leads to a more satisfactory rationalisation of the reaction pathway. Differences in OER catalytic activities between Ni electrodes subjected to different pre-treatments were postulated to arise principally from electrochemical considerations (i.e. the relative amounts of  $\beta$ -

NiOOH to  $\gamma$ -Ni produced by the electrochemical pre-treatment) as opposed to physical (surface roughness) reasons. The identification of  $\beta$ - $\beta$  cycle material as “the right type of oxide” for the OER is confirmed (Figs. 5 & 6).

#### ACKNOWLEDGEMENT

The authors are grateful for the financial support of Enterprise Ireland Grant Number SC/2003/0049, IRCSET Grant Number SC/2002/0169 and the HEA-PRTL Program.

#### Notes and References

‡a Since potentials are measured with respect to a Hg/HgO, 1M NaOH reference electrode, it is appropriate to plot polarisation curves on an oxygen overpotential,  $\eta$ , scale (see equation (1)) where all the data has been recorded in 1.0 M NaOH solution. This approach is useful for comparing the OER catalytic performance of an electrode, with that of other anodes reported in the literature. When electrolyte solutions other than 1.0 M NaOH are involved we continue to plot the data in terms of the potential,  $E$ , vs. Hg/HgO, 1M NaOH.

1. D.E. Hall, *J. Electrochem. Soc.*, 130 (1983) 317.
2. K. Kinoshita, *Electrochemical Oxygen Technology*, Wiley-Interscience, New York, 1992, chapter 2, pp. 78-99.
3. P.W.T. Lu and S. Srinivasan, *J. Electrochem. Soc.*, 125(1978) 1416.
4. B.E. Conway and P.L. Bourgault, *Can. J. Chem.*, 37(1959) 292.
5. B.E. Conway and P.L. Bourgault, *Trans. Faraday Soc.*, 58(1962) 593.
6. R.D. Armstrong, G.W.D. Briggs and E.A. Charles, *J. Appl. Electrochem.*, 18(1988) 21.
7. E.B. Castro, S.G. Real and L.F. Pinheiro Dick, *Int. J. Hydrogen Energy*, 29(2004) 255.
8. A.I. Krasil'shchikov, *Zh. Fiz. Khim.*, 37(1963) 531.
9. J.P. Hoare, *The Electrochemistry of Oxygen*, Interscience, New York, 1968, pp. 82-91, 284-291.
10. G. Bronoel and J. Reby, *Electrochim. Acta*, 25(1980) 973.
11. C. Bocca, A. Barbucci and G. Cerisola, *Int. J. Hydrogen Energy*, 23(1997) 247.
12. X. Wang, H. Luo, D-R Zhou, H. Yang, P.J. Sebastian and S.A. Gamboa, *Int. J. Hydrogen Energy*, 29(2004) 967.
13. Y. Zhang, X. Cao, H. Yuan, W. Zhang and Z. Zhou, *Int. J. Hydrogen Energy*, 24(1999) 529.
14. A.M. Fundo and L.M. Abrantes, *Russian J. Electrochem.*, 42(2006) 1291.
15. J.O'M. Bockris and T. Otagawa, *J. Phys. Chem.*, 87(1983) 2960.
16. R.F. Scarr, *J. Electrochem. Soc.*, 116(1969) 1526.
17. L.D. Burke and T.A.M. Twomey, *J. Electroanal. Chem*, 162(1984) 101.
18. A. Seghioer, J. Chevalet, A. Barhoun and F. Lantelme, *J. Electroanal. Chem*, 442(1998) 113.
19. J.F. Wolf, L-S. Yeh and A. Damjanovic, *Electrochim. Acta*, 26(1981) 409.
20. R.A. Robinson and R.H. Stokes, *Electrolyte Solutions*, Revised 2<sup>nd</sup> Ed. Butterworth & Co. Ltd., London, 1965, pp. 492.
21. G.J. Hills and D.J.G. Ives, in *References Electrodes*, D.J.G. Ives and G.J. Janz, Eds., Academic Press, New York, 1961, chapter 7.
22. D.T. Sawyer, A. Sobkowiak and J.L. Roberts Jr., *Electrochemistry for Chemists, Second Edition*, Wiley-Interscience, New York, 1995, chapter 5.
23. J.P. Hoare, *The Electrochemistry of Oxygen*, Interscience, New York, 1968, chapter 2.
24. H. Willems, A.G.C. Kobussen, J.H.W. De Wit and G.H.J. Broers, *J. Electroanal. Chem*, 170(1984) 227.

25. M.R. Gennero De Chialvo, A.C. Chialvo, *Electrochim. Acta*, 35(1990) 437.
26. J.C.K. Ho and D.L. Piron, *J. Electrochem. Soc.*, 142(1995) 1144.
27. J.C.K. Ho and D.L. Piron, *J. Appl. Electrochem.*, 26(1996) 515.
28. S. Gottesfeld and S. Srinivasan, *J. Electroanal. Chem.*, 86(1978) 89.
29. J.L. Weininger and M.W. Breiter, *J. Electrochem. Soc.*, 110(1963) 484.
30. G.W.D. Briggs, in *Electrochemistry - Vol 4, Specialist Periodical Reports*, The Chemical Society, London, 1974, chapter 3, pp. 33-59.
31. J. McBreen, in *Handbook of Battery Materials*, J.O. Besenhard, Ed., Wiley-VCH, Weinheim, 1999.
32. H. Bode, K. Dehmelt and J. Witte, *Electrochim. Acta*, 11(1966) 1079.
33. R. Barnard, C.F. Randell and F.L. Tye, *J. Appl. Electrochem.*, 10(1980) 109.
34. C. Greaves and M.A. Thomas, *Acta Cryst.*, B42(1986) 51.
35. S. Le Bihan and M. Figlarz, *J. Cryst. Growth*, 13/14(1972) 458.
36. M. Wehrens-Dijkema and P.H.L. Notten, *Electrochim. Acta*, 51(2006) 3609.
37. M. K. Carpenter and D.A. Corrigan, Abstract No. 490 of papers presented at the Atlanta Meeting of the Electrochem. Soc., May 15-20, 1988, p. 700.
38. M.J. Madou and M.C.H. McKubre, *J. Electrochem. Soc.*, 130(1983) 1056.
39. S.A. Aleshkevich, E.I. Golovchenko, V.P. Morozov and L.N. Sagoyan, *Soviet Electrochem.*, 4(1968) 530, 1117.
40. M.P. Brandon, Ph.D. Thesis, University of Dublin, Trinity College, 2008.
41. M.R. Gennero De Chialvo and A.C. Chialvo, *Electrochim. Acta.*, 33(1988) 825.
42. A.G.C. Kobussen, H. Willems and G.H.J. Broers, *J. Electroanal. Chem.*, 142(1982) 85.
43. A.G.C. Kobussen and C.M.A.M. Mesters, *J. Electroanal. Chem.*, 115(1980) 131.
44. M.E.G. Lyons and M.P. Brandon, in preparation.
45. R.D. Armstrong and M. Henderson, *J. Electroanal. Chem.*, 39(1972) 81.
46. B.E. Conway and T.-C. Liu, *Langmuir*, 6(1990) 268.
47. E.B. Castro, C.A. Gervasi and J.R. Vilche, *J. Appl. Electrochem.*, 28(1998) 835.
48. G. Wu, N. Li, D-R. Zhou, K. Mitsuo and B-Q. Xu, *J. Solid State Chem.*, 177(2004) 3682.
49. D.A. Harrington and B.E. Conway, *Electrochim. Acta.*, 32(1987) 1703.
50. B.E. Conway and E. Gileadi, *Trans. Faraday Soc.*, 58(1962) 2493.
51. W. O'Grady, C. Iwakura, J. Huang and E. Yeager, in *Proceedings of the Symposium on Electrocatalysis*, M.W. Breiter, ed., The Electrochemical Society Inc., Pennington, NJ, 1974, p286.
52. M.E.G. Lyons and L.D. Burke, *J. Chem. Soc., Faraday Trans. 1*, 83(1987) 299.
53. E.J.M. O'Sullivan and L.D. Burke, *J. Electrochem. Soc.*, 137(1990) 466.
54. L.D. Burke and M.E.G. Lyons, in *Modern Aspects of Electrochemistry, Vol. 18*, R.E. White, J.O'M. Bockris and B.E. Conway, Eds., Plenum Press, New York, 1986, p169.
55. A. Damjanovic, A. Dey and J.O'M. Bockris, *Electrochim. Acta.*, 11(1966) 791.
56. M.E.G. Lyons and M.P. Brandon, to be submitted to this journal, part 3 of the present series.
57. J. Willsau, O. Wolter and J. Heitbaum, *J. Electroanal. Chem.*, 195(1985) 299.
58. S. Trasatti and O.A. Petrii, *Pure & Appl. Chem.*, 63(1991) 711.
59. A.I. Fedorova and A.N. Frumkin, *J. Phys. Chem. USSR*, 27(1953) 247.
60. A.N. Frumkin, *J. Res. Inst. Catalysis (Hokkaido Univ.)*, 15(1967) 61.
61. J.O'M. Bockris and T. Otagawa, *J. Electrochem. Soc.*, 131(1984) 290.
62. V.D. Jovic, Gamry Instruments, Application Note, Determination of the correct value of  $C_{dl}$  from the impedance results fitted by the commercially available software, Gamry Instruments, 2003.
63. L.M. Da Silva, V.A. Alves, M.A.P. Da Silva, S. Trasatti and J.F.C. Boodts, *Electrochim Acta*, 42(1997) 271.